Review

Recent Progress on the Materials of Oxygen Ion-Conducting Solid Oxide Fuel Cells and Experimental Analysis of Biogas-Assisted Electrolysis over a LSC Anode

Christos Drosakis [1], Savvas Douvartzides [1], Costas Athanasiou [2] and Georgios Skodras [1,*]

[1] Department of Mechanical Engineering, School of Engineering, University of Western Macedonia, 50100 Kozani, Greece; chrisdro@windowslive.com (C.D.); sdouvartzidis@uowm.gr (S.D.)
[2] Department of Environmental Engineering, Democritus University of Thrace, 67100 Xanthi, Greece; kathan@env.duth.gr
* Correspondence: gskodras@uowm.gr; Tel.: +30-2461-056-662

Abstract: In this work, the recent achievements in the application of solid oxides fuel cells (SOFCs) are discussed. This paper summarizes the progress in two major topics: the materials for the electrolytes, anode, and cathode, and the fuels used, such as hydrocarbon, alcohol, and solid carbon fuels. Various aspects related to the development of new materials for the main components of the materials for electrocatalysts and for solid electrolytes (e.g., pure metals, metal alloys, high entropy oxides, cermets, perovskite oxides, Ruddlesden–Popper phase materials, scandia-stabilized-zirconia, perovskite oxides, and ceria-based solid electrolytes) are reported in a coherent and explanatory way. The selection of appropriate material for electrocatalysts and for solid electrolyte is crucial to achieve successful commercialization of the SOFC technology, since enhanced efficiency and increased life span is desirable. Based on the recent advancements, tests were conducted in a biogas-fueled Ni-YSZ/YSZ/GDC/LSC commercial cell, to elucidate the suitability of the LSC as an anode. Results obtained encourage the application of LSC as an anode in actual SOFC and SOFEC systems. Thus, H_2-SOFC demonstrated a satisfying ASR value, while, for biogas-assisted electrolysis, the current values slightly increased compared to the methane-SOFEC, and for a 50/50 biogas mixture of methane and carbon dioxide, the corresponding value presented the higher increase.

Keywords: solid oxide fuel cell; perovskite electrode; electrolyte materials; biogas

1. Introduction

Climate change and environmental pollution, along with price volatility, geopolitical risks, and population explosion (particularly in the developing world) urges the detachment from fossil fuels (coal, diesel oil, and natural gas). To achieve that, the exploitation of renewable energy sources (solar, wind, geothermal, biomass, biofuels, green hydrogen, etc.), in high-efficiency power generation/conversion systems has emerged as the only reliable strategy to secure energy supply towards a sustainable future [1,2].

Among the various energy conversion and storage systems, fuel cells hold a special position for their high efficiency in converting the chemical energy into electricity, environmental sustainability with low or even zero greenhouse gas emissions, fuel flexibility, and versatility for utilization in a wide range of stationary (industrial, building, residential, etc.) and mobile (automobiles, trains, aircrafts, etc.) applications [3–6].

Solid oxide fuel cells (SOFCs) constitute a certain category of fuel cells which operate at intermediate and high temperatures (400–1000 °C) and are widely regarded as the most promising for industrial and building applications. This is attributed to their high tolerance in fuel impurities which permits operation with various opportunity fuels (hydrogen, syngas, pyrolytic or gasification gases, biogas, biomethane, natural gas, hydrocarbons, bioalcohols, ammonia, etc.) either indirectly after their preliminary external steam reforming

or directly by exploiting their ability to facilitate the internal steam reforming of many fuels onto their anode electrocatalysts [7–11]. As in all fuel cells, SOFCs execute the electrochemical conversion of the chemical energy of the fuel directly into electricity, and, hence, they are not heat engines, and they are not restricted by the Carnot cycle efficiency limitations [12]. This practically means that SOFCs' electrical efficiencies might be as high as about 60%. If the accompanied heat production is also usefully exploited, then high heat and power cogeneration efficiencies might exceed 90%. Due to above advantages, SOFCs are suitable for mini-cogeneration units and large-scale power generation or combined heat and power (CHP) cogeneration plants with superior efficiencies compared to competitive gas turbine and Rankine cycle plants [6,10,11].

Most SOFCs are constructed with a solid ceramic electrolyte known as yttria-stabilized-zirconia (YSZ) which exhibits high conductivity of oxygen anions (O^{2-}) at the typical high temperatures of operation [13,14]. For the specific YSZ electrolyte, a structure of 8 mol.% yttria (Y_2O_3) in zirconia (ZrO_2) was found to maximize the required O^{2-} anion conductivity and is usually preferred. The high operating temperatures increase the electrode reaction kinetic rates and result in increased tolerance to fuel impurities, fuel flexibility, functionality with fuel internal reforming, and the possibility for operation with cheap electrode materials such as transition metals, Ni-based alloys, Ni-YSZ cermets, and perovskite oxides.

Thus, high operation temperatures reduce the construction cost in comparison to low temperature fuel cells which rely heavily on expensive noble metal electrocatalysts but pose challenges on the stability of the materials and the durability of the construction elements under much more severe thermal stresses and combined heating and corrosion deterioration effects. Towards the successful commercialization of SOFCs, challenges such as a reduction in material and construction costs, increased durability for long-time operation, slow dynamic response, and load tracking ability during transient operation in power demand should be confronted. Furthermore, the susceptibility of their ceramic elements to mechanical or thermal (during sudden temperature change) fracture, and the fuel cell stacking methods should be improved, and issues of safety and of routine maintenance should be resolved [10,11,15,16].

This work focuses on the most promising outputs of recent research on the development of novel materials for the main components of the anode, cathode, and oxygen conducting solid electrolytes of various SOFCs using hydrogen, hydrocarbons, alcohols, and solid carbon as anode fuels. These research results are critically discussed to highlight the progress achieved so far on the race for better electrocatalysts and electrolytes in terms of all the required SOFC performance criteria. Furthermore, experimental results of the electrochemical performance of a Ni-YSZ/YSZ/GDC/LSC biogas-assisted electrolysis fuel cell are presented, investigating the overall electrochemical performance under different biogas mixtures.

Working Principle of SOFCs

A typical SOFC consists of a dense layer of solid ceramic electrolyte (usually YSZ) which is sandwiched between the anode and cathode electrodes/electrocatalysts (Figure 1). The two electrodes are composed of materials with high catalytic activity for the corresponding oxidation (anode) and reduction (cathode) electrochemical semi-reactions, high electrical conductivity, and high porosity that facilitates the maximization of the so-called gas–electrode–electrolyte "three phase boundary" (TPB) where the electrochemical redox reactions take place [14].

In a typical SOFC operation, the initial reaction takes place at the cathode. The oxygen atoms react with the free electrons coming from the external electrical circuit and are reduced to oxygen anions. These anions migrate through the solid oxide electrolyte to the anodic electrode where they electrochemically oxidize the fuel.
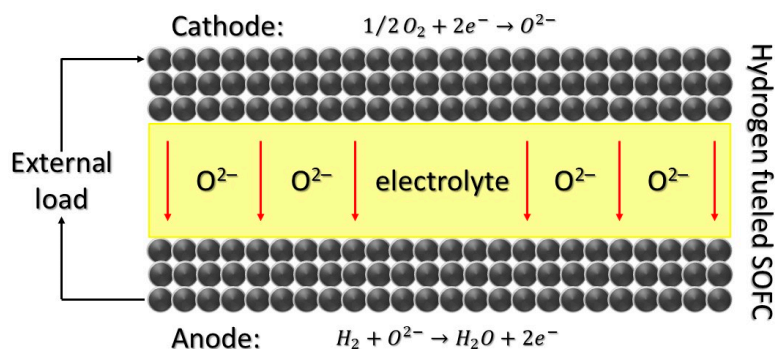
Figure 1. Schematic diagram of a hydrogen-fueled SOFC [14].

The fuel is supplied to the anode while oxygen (mainly in the form of air) enters into the cathode. During operation, the oxygen atoms arriving at the cathode electrocatalyst react with the free electrons coming from the external electrical circuit and form oxygen anions (Equation (1)). These, in turn, migrate through the electrolyte layer to the anode and react with the fuel as shown in the case of fuel hydrogen in Equation (2) [14].

$$\frac{1}{2}O_2 + 2e^- \longrightarrow O^{2-} \tag{1}$$

$$H_2 + O^{2-} \longrightarrow H_2O + 2e^- \tag{2}$$

Electrical energy production is achieved by the flow of electrons through the external circuit connected to an external load, typically made of metals that demonstrate high temperature resistance [13]. In the case of a hydrocarbon fuel under theoretically ideal conditions, anode oxidation reaction leads to the production of both water and carbon dioxide as shown in Equation (3) [17], below.

$$C_x H_{2x+2} + (3x+1)O^{2-} \rightarrow xCO_2 + (x+1)H_2O + (6x+2)e^- \tag{3}$$
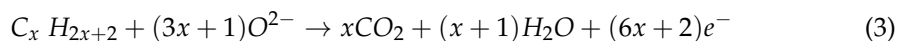
Oxygen ion migration through the electrolyte is driven by oxygen's partial pressure difference across the electrolyte and takes place at a rate which depends on the operation temperature and the ionic conductivity of the specific electrolyte. To avoid parasitic voltage and efficiency losses, the electrolyte must ideally operate as an electrical insulator.

Although hydrogen is the most efficient fuel for fuel cells, it is not commonly employed due to several complications and strict requirements regarding its production, transport, and storage, along with the associated costs [18]. As a result, SOFCs are usually considered for operation with various other opportunity fuels such as syngas (a mixture of H_2 and CO), pyrolytic or gasification gases, biogas, biomethane, natural gas, hydrocarbons, bio-alcohols, and ammonia [19–21].

2. Advances in Materials

2.1. Electrolyte

The electrolyte is at the core of the fuel cell, sandwiched between the two electrodes, and its selection has a considerable impact on the SOFC efficiency and performance [22–25]. Its primary function is to conduct oxide ions (O^{2-}) from cathode to anode. Furthermore, it can serve as a support of the two electrolytes on the so called "electrolyte supported SOFCs", as for example in the fabrication of planar designs at high temperatures. Also, the selection of the electrolyte materials is quite demanding to ensure the viability of the fuel cell. These must have high ionic conductivity (0.01–0.1 S/cm for 1–100 µm thickness) along with high electronic insulation, gas tightness with minimal porosity, and, most importantly, mechanical, thermal, and chemical stability under extreme conditions, since an electrolyte is exposed at high temperatures and different reducing and oxidizing environments. The thermal expansion coefficient (TEC) of the electrolyte must be compatible with the corresponding TECs of the anode and cathode materials to avoid the formation of cracks.

Finally, since ohmic losses increase with the electrolyte's thickness, electrolytes must be manufactured in the form of thin layers and the cost of the material together with the cost of the manufacturing process are crucial parameters that must be taken under consideration.

Over the last few decades, a wide range of materials have been researched in order to meet the aforementioned requirements and advance SOFC technology. YSZ is the most frequently used electrolyte due to its excellent chemical and thermal stability and low fabrication cost compared to other SOFC electrolytes [26]. The ionic conductivity of zirconia electrolytes is dependent on both the doping oxide and its concentration. For YSZ, the highest conductivity is observed at 8 mol%, since Yttria at the specific concentration creates a favorable balance of oxygen vacancies and a stable cubic structure that maximizes the mobility of oxygen ions. Compositions with higher or lower concentrations can lead to reduced conductivity due to the clustering of defects or phase separation. The high ionic conductivity of approximately 0.12 S/cm and 0.02 S/cm at 1000 °C and 800 °C, respectively, is the reason that YSZ is considered to be the most prevalent electrolyte for high-temperature SOFCs [27]. However, for operating temperatures below 600 °C, YSZ exhibits low ionic conductivity (0.001 S/cm) and, consequently, does not meet the requirements for intermediate-temperature SOFCs (IT-SOFCs), which have sparked major research interest nowadays.

An alternative electrolyte material that can be efficiently used in IT-SOFCs is scandia-stabilized zirconia (SSZ) which was found to exhibit higher ionic conductivity than YSZ at 500 °C [28,29]. Badwal et al. [30] found also that SSZ's with 8–9% doped scandia content exhibit superior mechanical stability and ion conductivity than the traditional YSZ electrolyte. However, a major hindrance to the commercialization of the SSZ electrolyte is the scarcity of scandium-rich minerals, along with the complexity of the procedures needed for their extraction and fabrication which, in turn, significantly increase the overall cost. In addition, in zirconia-based electrolytes, cathodes containing La, Ba, etc., can react with YSZ, resulting in a substantial increase in the polarization and ohmic losses of the cell. As a result, for all zirconia-based electrolytes, the range of appropriate cathode materials is rather limited.

ABO_3-type perovskites constitute a large category of oxides where A is an alkaline or lanthanum earth element, and B represents a transition metal element [31–34]. A group of materials of this category including $La_2M_{O2}O_9$, $LnBO_3$ perovskites (B = Sc, Y, Al), doped $LaGaO_{3-}$ perovskites, and brownmillerite-like phases ($A_2B_2O_5$) have demonstrated high oxygen ion conductivity at intermediate temperatures, making them suitable for IT-SOFC electrolyte materials [34].

The most researched perovskite material for IT-SOFC is $LaGaO_{3-}$. Ishihara et al. [35] discovered in 1994 that by partially substituting La and Ga with divalent strontium (Sr^{2+}) and magnesium (Mg^{2+}) ions, respectively, the produced perovskite-structured solid electrolytes (abbreviated as $La_{1-x}Sr_xGa_{1-y}Mg_yO_3$ or LSGM) exhibited high oxygen ion conductivity due to the creation of a considerable amount of oxygen vacancies generated in the perovskite's structure. The conductivity of LSGM at 750 °C is approximately 0.1 S/cm, which is very close to that of GDC or SDC electrolytes. Various studies [36,37] were conducted to determine the optimal doping combination for LSGM, and it was found that when x = 0.2 and y = 0.17, the value maximizes at 800 °C at approximately 0.18 S/cm. At 600 °C, the oxygen ion conductivity of the different LSGM doping amounts examined was at the region of approximately 0.03 S/cm, which is far superior to the respective value of the YSZ electrolyte at the same temperature.

However, despite the high ionic conductivity and chemical stability, LSGM's complex composition renders them susceptible to the emergence of secondary phases that negatively affect the conductivity [38]. Another challenge for these electrolytes is their low sinterability, as it is more difficult to attain dense LSGM electrolytes [27]. These challenging difficulties impede the application of LSGM in the commercial IT-SOFCs, and, as a response, considerable research is currently underway on the development of novel fabrications methods [39–41].

Another group of materials suitable for SOFC are ceria-based electrolytes. CeO_2 has a cubic fluorite structure that maintains stability from room temperature to its melting point. Since pure CeO_2 has limited oxygen vacancies, ceria is doped with trivalent metal oxides to increase their number and thus improve oxygen ion conductivity. At temperatures below 800 °C, the conductivity of ceria-based electrolytes exceeds that of YSZ electrolyte, the difference being larger at lower temperatures [42]. Studies have validated that as the ionic radius of the trivalent dopant is closer to the respective value of Ce^{4+}, the expected conductivity increases [43]. Among this category, gadolinium oxide-doped ceria (GDC) and samarium oxide-doped ceria (SDC) have high ionic conductivity and are used in SOFCs [44]. The reported conductivities are 0.061 S/cm and 0.067 S/cm for SDC and GDC, respectively, at the operating temperature of 750 °C.

Furthermore, most of the ceria-based electrolytes have the advantage of demonstrating good chemical compatibility with many cathodic electrodes such as LSCF and BSCF in the intermediate temperature range. A major limitation for ceria-based electrolytes is that under a reducing environment (low partial oxygen pressure), Ce^{4+} ions are reduced to Ce^{3+}. This leads to a partial electronic conductivity, which in turn causes a decrease in the open circuit voltage (OCV) and the overall efficiency of the SOFC [45]. Zhang et al. [46] investigated this phenomenon for thin-film SDC electrolytes. This problem can be addressed by applying a thin YSZ layer between the electrolyte and the anode.

2.2. Anode

The anode electrode executes the electrochemical oxidation of the supplied fuel into water and carbon dioxide while, simultaneously, it collects the electrons produced and delivers them to the external circuit. Anode materials must exhibit high electronic conductivity and adequate electrocatalytic activity to promote the associated fuel oxidation reactions. They must be chemically stable under the extreme-reducing and high-temperature environments, and they must be thermally and chemically compatible to the materials of the electrolyte and cathode, especially in terms of their TEC. Regarding microstructure, they should have a fine particle size and a large TPB to maximize the oxidation reaction rates and, consequently, the efficiency of the cell. Finally, anodes must have high porosity to accommodate efficient gas transportation together with acceptable tolerance to fuel impurities, such as sulfur, which may lead to serious degradation of the SOFC performance [22–24,47].

Ni-YSZ cermet anodes are one of the most widely used anode materials. They were first introduced by Liu et al. [48] in 1995. Metal Ni is plentiful with lower relative pricing than other metals used for anode electrodes, and the Ni-YSZ cermet anode configuration provides sufficient ionic conductivity and increases the reaction area of the TPB. This cermet combination also ensures the structural stability of the SOFC since it lowers the TEC of nickel, which for pure Ni is relative higher than the respective TEC values of the electrolytes, to a degree that is compatible with the used electrolytes [49]. Ni-YSZ cermet is the most promising material for hydrogen-fueled SOFC anode fabrication.

Despite the mentioned advantages, Ni is prone to carbon deposition and has low sulfur tolerance when using hydrocarbon fuels. As a result, some areas of the TPB are deactivated, and the overall performance and endurance of the SOFC is compromised [17,49]. Furthermore, it is observed that at prolonged operation periods, Ni particles are prone to sintering, leading to the agglomeration and coarsening of their particles and consequently to the drastic reduction in the catalytic activity of the anode [50]. To address these challenges, researchers focused on alternative porous anode materials such as perovskite structures and metal ceramic composites.

Copper was found to exhibit high resistance to carbon deposition and has been examined extensively as a possible anode material. Since Cu has a lower melting point than Ni, its fabrication with the traditional sintering method is impractical, and new methods, such as wet impregnation, were employed [51,52]. Although it provides an electronic conduction path, it has low electrochemical activity, a drawback that can be addressed by adding ceria oxide catalyst to enhance the latter. Lu et al. [53] examined the current-voltage

and impedance characteristics of SOFCs with Cu-SDC and Au-SDC anodes with SDC electrolyte under H_2 and n-butane anodic fuels at 650 °C. It was found that both metals exhibit poor catalytic activity for C-H and C-C bond breaking and, consequently, are stable for environments of hydrocarbon fuels.

Kim et al. [54] tested different Cu-Ni alloys (0%, 10%, 20%, 50%, and 100% Ni) as anodes with dry CH_4 as fuel at 800 °C. The results demonstrated that these alloys greatly suppressed carbon deposition over the anode in comparison to pure Ni. In terms of power density, a significant increase over time was evident due to the enhanced electronic conductivity of the anode. Costa-Nunes et al. [55] attempted a comparison of the performance of SOFCs with a Cu-CeO$_2$-YSZ anode to SOFCs with Ni-YSZ anodes using H_2, CO, and syngas as possible fuels. SOFCs with Cu-CeO$_2$-YSZ anode electrodes exhibited significant improvement in terms of performance compared to these with Ni-YSZ cermets. For operation at 700 °C, the SOFCs with the Ni-YSZ anode yielded maximum power densities of 136, 73, and 120 mW/cm^2 with H_2, CO, and syngas fuels, respectively, while the SOFCs with a copper composite anode exhibited greater (about 305 mW/cm^2) or similar power densities at the same operating conditions.

Furthermore, the role of cobalt addition in Cu-CeO$_2$-YSZ composites was also investigated. A substantial enhancement in the catalytic activity of the Co-Cu-CeO$_2$-YSZ cermet anode was observed as the SOFC yielded maximum power densities up to 310 mW/cm^2 with H_2 and 370 mW/cm^2 with CO fuels. More recently, Wang et al. [56] managed to fabricate (Cu, Sm) CeO$_2$ anodes with in situ exsolution via the reduction method. The maximum amount of Cu nanoparticles that was doped into the SDC electrolyte was approximately 10 mol%. The resulting anode exhibited improved conductivity and catalytic activity with dry methane as the fuel, and the attained maximum power density of the SOFC was 404.6 mW/cm^2 at 600 °C. The corresponding maximum power density for natural gas as a fuel was 415.2 mW/cm^2.

Perovskite oxides have been widely used as electrode and electrolyte materials in SOFCs [31–33]. The bulk of these oxides exhibit both high electronic and oxygen ionic conductivities, a property that can be defined as "mixed ionic–electronic conductivity" (MIEC). These perovskites have significantly larger TPB areas leading to increased cell performance [57]. However, as compared to the widely used Ni-YSZ cermet, MIEC perovskite oxides exhibit lower electrical conductivity, power density, and catalytic activity, facts that have triggered extensive remedy research efforts during the last years.

Tao and Irvine [40] developed a La$_{0.75}$Sr$_{0.25}$Cr$_{0.5}$Mn$_{0.5}$O$_3$ anode that demonstrated good resistance to carbon deposition and adequate stability at high temperatures. Zhu et al. [58] fabricated an LSCrM-YSZ anode composite by impregnating La$_{0.75}$Sr$_{0.25}$Cr$_{0.5}$Mn$_{0.5}$O$_3$ into a YSZ scaffold. The maximum power density of the cell, for dry H_2 as a fuel at 850 °C, was 198 mW/cm^2, but the complexity of the fabrication procedure and the lack of reproducibility were limiting factors. Based on the latter limitation, Zung et al. [59] used a polymeric complex resin method to fabricate an LSCrM-YSZ nanocomposite anodic electrode. The enhanced distribution of particles resulted in better performances than the mechanically mixed LSCrM-YSZ anode. The maximum power density for the nanocomposite anode was 177 mW/cm^2 while the respective value for the mechanically mixed LSCrM-YSZ anode was 136 mW/cm^2 at the operating temperature of 850 °C.

Another approach followed was the substitution of Mn with an Fe dopant. Tao and Irvine [60] examined the electrochemical performance of an La$_{0.75}$Sr$_{0.25}$Cr$_{0.5}$Mn$_{0.5}$O$_{3-\delta}$ anode at 900 °C while supplying an anode with CH_4 and O_2 in different molar ratios. For an equimolar mixture of CH_4 and O_2 at the anode, the observed methane conversion was 11% while the maximum conversion of methane (96%) was observed for a CH_4/O_2 molar ratio equal to 1:2. Regarding the anode polarization resistance, the values of 1.79 and 1.15 Ωcm^2 were obtained for wet 5% H_2 and wet H_2, respectively, at 850 °C. Fowler et al. [61] fabricated La$_{1-x}$Sr$_x$Cr$_x$Fe$_{1-x}$O$_{3-\delta}$ powders according to a solid-state reaction method and tested five different anode compositions. Among these, La$_{0.33}$Sr$_{0.67}$Cr$_{0.33Fe0.67}$O$_{3-\delta}$ exhibited the lowest anodic polarization resistance of 0.275 Ωcm^2 for an anodic supply

of wet H_2 at 800 °C. This was significantly lower compared to the reported value of the $La_{0.75}Sr_{0.25}Cr_{0.5}Mn_{0.5}O_{3-\delta}$ anode of Tao and Irvine [60] under the same conditions.

Following the previous research, Aliotta et al. [62] evaluated a series of $La_{1-x}Sr_xCr_{1-y}Fe_yO_{3-\delta}$ (x = 0.1, 0.15, and 0.2 while y = 0, 0.3, and 0.5) catalysts as anodes in direct methane-fed SOFCs. They deployed different mixtures of CH_4 and He and found that they could stimulate both total and partial methane oxidation at temperatures below 700 °C and between 850 and 950 °C, respectively. Among the examined composites, $La_{0.9}Sr_{0.1}Cr_{0.7}Fe_{0.3}O_{3-\delta}$ exhibited excellent catalytic activity to oxidize H_2S and CH_4, rendering them suitable fuels for application in IT-SOFCs.

Sun et al. [63] examined the effect that different concentrations of doped Ce into LSCF have on the electrochemical performance of the cells. The anode doped with 5% Ce ($La_{0.65}Sr_{0.3}Ce_{0.05}Cr_{0.5}Fe_{0.5}O_{3-\delta}$) exhibited an anodic polarization resistance of 0.25 Ωcm^2 at 800 °C, which was four-times lower compared to the corresponding value of the non-doped LSCF and approximately 40% lower than that for the cell with an anode doped with 10% Ce. Furthermore, the $La_{0.65}Sr_{0.3}Ce_{0.05}Cr_{0.5}Fe_{0.5}O_{3-\delta}$ cell exhibited lower activation polarization resistance. The improved performance was attributed to the presence of an increased number of oxygen vacancies in the lattice, leading to higher oxygen mobility.

The advancements in fabrication processes have led to the development of more effective perovskite anodes. In situ exsolution is one of these methods, which results in better-dispersed nanoparticles and larger specific surface areas that promote the involved catalytic reactions. Sun et al. [64] exploited this method to fabricate an A-site deficient $La_{0.6}Sr_{0.3}Cr_{0.85}Ni_{0.15}O_{3-\delta}$ anode which exhibited satisfactory electrochemical performance with a maximum power density of 460 mW/cm^2 and a maximum current density of approximately 1200 mA/cm^2 under operation with a supply of 5000 ppm H_2S-H. Fowler et al. [65] synthesized and assessed the perovskite compounds $La_{0.33}Sr_{0.67}Cr_{1-x-y}Fe_xRu_yO_{3-\delta}$ (LSCr-FeRu, x = 0.62, 0.57, and 0.47; y = 0.05, 0.14, and 0.2, respectively) with a GDC electrolyte and with humidified H_2 as a fuel at 800 °C. The reported anodic polarization resistances were 0.29 Ωcm^2, 0.235 Ωcm^2, and 0.195 Ωcm^2, respectively, indicating that the doping of Ru and Fe resulted in improved electrochemical performance compared to anode compositions doped exclusively with one of the aforementioned elements.

In addition, the substituted Ru nanoparticles increased the active dissociation of H_2 molecules to hydrogen atoms which subsequently migrate from the Ru metallic surface to the proximate oxide surface due to the hydrogen spillover phenomenon leading to an enhanced hydrogen dissociative adsorption rate and thus changed the rate-limiting process from the former to the electrochemical oxidation of H_2. More recently, Wang et al. [66] synthesized an Ru and Ce co-doped perovskite oxide $La_{0.6}Ce_{0.1}Sr_{0.3}Fe_{0.95}Ru_{0.05}O_{3-\delta}$ as anode at a symmetrical LSCFR-CGO/LSGM/LSCFR-CGO cell. The cell exhibited a maximum power density of 904 mW/cm^2 for an anodic supply of 97% H_2—3% H_2O at 800 °C. This performance was attributed to the exsolved metallic Ru nanoparticles in the anode. Peng et al. [67] prepared an SMM-infiltrated NiO-SDC composite anode via in situ exsolution. The maximum power densities of the fabricated electrolyte-supported symmetrical SOFC with an SMM/NiO-SDC electrode reached 245 and 183 mW/cm^2 at 800 °C operating in wet CH_4 and C_2H_5OH fuels, respectively. The results indicated stable operation in hydrocarbon fuel with enhanced electrochemical activity and carbon deposition resistance.

Among the promising materials for anodes, strontium titanate-based perovskites have gathered a considerable amount of research over the last years. They exhibit good stability under oxidizing and reducing environments, and doping $SrTiO_3$ overcomes the insulating properties of undoped strontium titanates and improves its electrochemical properties. The nature of the dopant strongly affects critical parameters of the perovskite such as sinterability, conductivity, and redox properties [68]. Park and Choi [69] fabricated an Ni-doped $La_{0.2}Sr_{0.8}Ti_{0.9}Ni_{0.1}O_{3-\delta}$ (LSTN) anode which was calcined at 1300 °C for 10 h. The examined cell of LSTN/ScSZ/LSCF-GDC exhibited an anode polarization resistance of 1.66 Ωcm^2 and a maximum power density of 150 mW/cm^2 with humidified H_2 fuel at

800 °C. The relative low peak power was attributed to the thickness of the electrolyte and the overall low anodic performance.

Sun et al. [70] prepared a lanthanum-doped strontium titanate-based perovskite with Ni and Ce as dopants (LSCNT) using a modified sol–gel method. The LSCNT anode showed improved electrochemical performance in 5000 ppm H_2S/H_2 with a maximum power density of 660 mW/cm^2 at 900 °C. Yoon and coworkers [71] investigated the effect of Ru doping into $La_{0.4}Sr_{0.6}TiO_{3-\delta}$ ($La_{0.4}Sr_{0.6}Ti_{1-x}Ru_xO_{3-\delta}$ for x = 0.02 and 0.05) (LSTR). The results indicated that under a reducing atmosphere, an amount of Ru nanoparticles was detected at the LSTR surface, which decreased the total electrical conductivity from 343.9 S/cm for pure LST to 202.9 S/cm for LSTR0.05 at 900 °C and increased the ionic conductivity from 0.0020 S/cm for pure LST to 0.0028 S/cm for LSTR0.05 for the same temperature and H_2 as fuel. This behavior was attributed to the B site deficiency which in turn promoted the generation of more oxygen vacancies along with the reduction in Ti^{+3} concentration. The power densities also increased from 52 mW/cm^2 for LST-YSZ to 115 mW/cm^2 for LSTR0.05-YSZ.

In another study, Xu et al. [72] prepared a CeO_2-infiltrated $La_{0.3}Sr_{0.7}Ti_{0.3}Fe_{0.7}O_{3-\delta}$ anode composite (LSTF0.7) which improved the electrocatalytic activity of CO and H_2. At 850 °C, the peak power densities of the fabricated cell were 815 mW/cm^2 and 721 mW/cm^2 for an anodic supply of H_2 and CO, respectively. More recently, Sayagués et al. [73] proposed an $Sr_{1-x}La_xTiO_3$ anode (SLT where values of x are between 0 and 0.5). It was found that the fabricated anode was chemically compatible with YSZ. This specific cell exhibited a peak power density of 231 mW/cm^2 at 900 °C at an operating voltage of 550 mV. Furthermore, Cao et al. [74] successfully developed a titanium-doped lanthanum ferrite perovskite $La_{0.3}Sr_{0.7}Fe_{0.7}Ti_{0.3}O_{3-\delta}$ (LSFT). They reported that Ti and Fe cations promoted enhanced synergistic effects on the electrocatalytic activity and durability. The maximum power density for wet CH_4 as fuel at 850 °C was observed to be 0.121 W/cm^2.

Apart from the aforementioned perovskites, high-entropy alloys, which were introduced in 1995 by Yeh and Huang [75] have triggered a considerable amount of research over the last years. HEAs are alloys that contain at least five principal elements with atomic concentrations ranging between 5 and 35% that exhibit enhanced mechanical stability and catalytic properties due to their unique complex structure [76]. Under this concept, Chen et al. [77] prepared an $SrV_{1/3}Fe_{1/3}Mo_{1/3}O_3$ anode electrode abbreviated as SVFMO. The fabricated electrolyte-supported cell SFMO/LSGM/LSCF exhibited a maximum power density of 720 mW/cm^2 at an operating temperature of 850 °C with H_2 as the anodic fuel and a polarization resistance of 0.371 Ωcm^2. The results validated SVFMO as a promising anode electrode. Finally, Lee at al. [78] fabricated an HEA/GDC anode electrode consisting of 9.75 wt.% Ni and Mn, 13 wt.% Co, and 16.25 wt.% Cu and Fe in order to compare its electrochemical performance and stability to that of conventional Ni-GDC and Ni-YSZ in an SOFC with an ScSZ electrolyte and LSM-YSZ cathode for CH_4 fuel with an S/C = 2 and ambient air in a cathode at 750 °C. Although the obtained current density of 100 mA/cm^2, under a 600 mV operating potential, for the HEA/GDC catalyst was lower than the conventional Ni-based anodes examined (250 mA/cm^2), it remained stable under 30 h of operation without any decay while the latter anodes exhibited solid carbon formation and were eventually deactivated.

2.3. Cathode

The cathode is an essential part of any SOFC where the oxygen reduction semi-reaction (ORR) takes place. The oxygen in the supplied air undergoes electrochemical reduction into oxygen ions (O^{2-}) which, in turn, migrate through the electrolyte up to the anode [79]. Generally, the ORR activity at the air electrode depends on four consecutive stages which are namely (a) the transportation of oxygen in the porous cathode, (b) the adsorption and dissociation of O_2, (c) the transportation of oxygen anions (O^{2-}) along the cathodic surface, and (d) the incorporation of O^{2-} into the electrolyte [14].

Any cathode material must fulfill a series of design criteria in order to ensure the effective operation of an SOFC [80,81]. Cathodes must exhibit high catalytic activity for the ORR and high electrical conductivity. Furthermore, in order to avoid mechanical failures and cracking, it is essential that their TEC be close to the respective TECs of the electrolyte and anode, as well as to be chemically compatible with the electrolyte. The cathode must be stable under the oxidizing atmospheres of fabrication and operation and also suitably porous to ensure the gaseous exchange via the cathode between the cathode/electrolyte interface. Finally, identically to the anode materials, cathode materials should be inexpensive to promote SOFC commercialization. The development of IT and LT-SOFCs and the attention they attracted recently have also influenced the material selection, since a number of traditional cathodes that perform well under temperatures above 800 °C have shown limited functionality due to high polarization resistances as the operating temperature is reduced. Potential materials for cathodes include many categories such as single perovskites, double-layered perovskite structures, MIEC perovskites, and composite electrodes.

Lanthanum strontium-doped manganite (LSM) is the most commonly used cathode material worldwide, meeting the bulk of the aforementioned requirements for ensuring high SOFC performance. LSM presents good thermal and chemical stability, adequate catalytic activity in ORR, and high ionic conductivity [82]. Its TEC is similar to that of the YSZ electrolyte, and, therefore, the probability of mechanical failure of the cell due to the potential length mismatch between electrolyte and cathode under heating conditions is reduced. However, as the operating temperature decreases, the activation energy of the ORR increases, and, consequently, LSM becomes unsuitable for IT-SOFC applications [83]. In order to increase its performance, various methods were employed. In one of them, the LSM is mixed with YSZ. Kilner et al. [84] examined LSM-YSZ composite cathodes in order to compare their oxygen diffusivity with that of pure LSM. The results demonstrated that the composites were more electrochemically active due to the extended TPBs.

Park et al. [85] examined LSM/YSZ powders of LSM content varying from 80 wt.% to 25 wt.%, focusing on the polarization resistances of the cell. The cathode containing 50 wt.% LSM exhibited the lowest polarization resistance (R_p) of 0.315 Ωcm^2, and the maximum power of the cell was 791 mW/cm^2, a performance that was attributed to the increase in the TPB active sites. Su and coworkers [86] fabricated an LSM/YSZ composite cathode with vertically aligned nano-columns (VANs) using the pulsed laser deposition (PLD) method. The resulting composite cathode had an ASR value of 0.35 Ωcm^2 at 700 °C, two-times lower than the conventional screen-printed LSM/YSZ composite, while the maximum power density achieved by the cell was 0.32 W/cm^2 at the same temperature.

More recently, Wang et al. [87] developed a PdO/ZrO$_2$-infiltrated LSM/YSZ composite cathode and evaluated its performance in a temperature range of 650–750 °C with H$_2$ as fuel while the cathode was exposed to air. The co-infiltration significantly improved the electrochemical performance of the anode-supported cell compared to the conventional LSM/YSZ cathode as the maximum power density varied from 438 to 1207 mW/cm^2, whereas the corresponding values for the conventional cathode were below 500 mW/cm^2. The obtained results showed that the fabricated composite increased the amount of the absorbed oxygen, promoting the surface oxygen adsorption and diffusion.

Another approach to address the low performance of pure LSM was introduced by Wang et al. [88] who proposed the coating of the cathode surface with a current-collecting layer (CCL) to increase the electrochemical performance of the oxygen electrode. The CCL examined was a 15% Al$_2$O$_3$ which was added into LSM and then sandwiched between the LSM-YSZ layer and SUS 430 interconnect. The resulting cell with the aforementioned configuration exhibited an ASR of 0.0253 Ωcm^2, significantly lower than the corresponding value of pure LSM (0.0657 Ωcm^2), while the peak power density was slightly higher for the proposed CCL cathode. Apart from LSM, a lot of research efforts were focused on developing new materials that offer better conductivity and stability under the operating

temperature ranges of the IT- and LT-SOFCs. These can be divided into two main groups that are namely cobalt-based and cobalt-free materials.

Lanthanum strontium cobaltite (LSC) was also examined as a potential cathode material for use in IT-SOFCs due to its high electronic and ionic conductivities under reduced temperatures [89,90]. Wu et al. [91] focused on the physical properties of $La_{1-x}Sr_xCoO_{3-\delta}$ and specifically on the effect of the Sr doping over the phase formation of the perovskite. The sample with x = 0.4 exhibited the maximum conductivity of 2583 S/cm at 500 °C. However, the TEC of this perovskite is significantly larger than the corresponding values of the typical SOFC components, and this can lead to grave mechanical failures such as cracking and poor structural quality. More recently, Son et al. [92] tried to address these problems by fabricating an LSC-GDC composite cathode using the PLD method. The new composited had improved microstructural stability, and the porosity of the configuration was more controllable by altering the deposition pressure.

Strontium-doped lanthanum cobalt ferrite (LSCF) has gathered a considerable amount of research over the past years as a replacement for traditional cathode materials. Its electrical and ionic conductivities of 10^2 S/cm and 10^{-2} S/cm, respectively, along with its sufficient oxygen surface exchange coefficient compared to LSM materials, are important reasons that triggered further research [93]. The drawback of the TEC value mismatch can be addressed by fabricating a composite cathode containing both LSCF and electrolyte material. Murray et al. [94] have observed that by adding 50 vol% GDC to LSCF resulted into a significant reduction in R_p which was observed at 0.01 Ωcm^2 and 0.33 Ωcm^2 at 750 °C and 600 °C, respectively. Under the same perspective, Lou and coworkers [95] achieved a uniform coating of SSC which was deposited on the porous surface of an LSCF cathode via solution infiltration. The results confirmed that the performance of the cathode was improved along with a considerable reduction in cell degradation.

Shen et al. [96] examined the microstructure and electrochemical performance of three cathode materials, LSCF, BSCF, and SSCF, for determining their applicability in IT- and LT-SOFCs. At 300 °C, the LSCF demonstrated a peak conductivity of 176 S/cm, whereas the corresponding values for the other two materials ranged between 4 and 50 S/cm. Yang et al. [97] prepared a state-of-the-art SCT/LSCF-GDC cathode using a combined solution infiltration and co-calcination method for overlapping SCT on the surface of LSCF-GDC. The resulting composite cathode exhibited higher electrochemical performance and stability compared to the conventional LSCF-GDC cathode under an environment rich in Cr. In 2021, Moghadam et al. [98] successfully fabricated, using a modified sol–gel method, $La_{0.7}Sr_{1.3}Co_{1-x}Fe_xO_4$ (x = 0, 0.1, 0.3, 0.5) cathode catalysts. The substitution of Fe in Co sites caused a decrease in the electrical conductivity while the ORR activity of the $La_{0.7}Sr_{1.3}Co_{1-x}Fe_xO_4$ -CGO cells was improved.

Another cobalt-based material that has received extensive attention is $Ba_{1-x}Sr_xCo_{1-y}Fe_yO_{3-\delta}$ (BSCF) as it exhibits low polarization resistance in the intermediate temperature range [99]. However, at specific temperatures, BSCF decomposes due to cobalt ion oxidation which consequently leads to the creation of a two-phase mixture of perovskites. The solution to this problem is doping with other elements to stabilize it. Yang et al. [100] doped molybdenum into BSCF via the gel combustion method in order to produce a more stable composite cathode at 700 °C. The fabricated BSCFM cathode achieved a peak power density of 418 mW/cm² at 700 °C as a result of the improved catalytic performance for ORR. Zeng et al. [101] doped the B-site of BSCF with 4 mol% Zn. The prepared BSCFZ cathode showed improved catalytic activity and stability as the Zn doping increased the oxygen vacancy concentration. The maximum power density values for temperatures of 650 °C, 700 °C, and 750 °C were 250 mW/cm², 410 mW/cm², and 580 mW/cm², respectively, significantly increased by approximately 35~41% from the corresponding values of the BSCF cathode.

An interesting cathode candidate was introduced recently by Nie et al. [102]. By doping the A-site of $PrBa_{0.94}Co_2O_{5+\delta}$ with Ca ions, they developed a highly active $Pr_{0.7}Ca_{0.3}Ba_{0.94}Co_2O_{5+\delta}$ cathode suitable for IT-SOFCs operation. The Ca doping promoted the ORR activity, and the polarization resistance was as low as 0.027 Ωcm^2 at 700 °C. The enhanced perfor-

mance was attributed to high oxygen vacancies and fast oxygen exchange. The cathode-based button cell achieved a peak power density of 1114 mW/cm^2 at the same temperature and demonstrated significant long-term stability under all operation conditions. Chen et al. [103] recently managed to synthesize a novel Nb^{5+}-doped La$_{0.5}$Sr$_{0.5}$Co$_{0.8}$Cu$_{0.2-x}$Nb$_x$O$_{3-\delta}$ cathode and evaluated its performance. At 700 °C, the LSCCu$_{0.15}$Nb$_{0.05}$O$_{3-\delta}$ demonstrated an R$_p$ value of 0.065 Ωcm^2, and the maximum power density for the NiO-GDC/GDC/LSCCNb cell was 518 mW/cm^2. The catalyst exhibited excellent stability and consequently validated the assumption that it is a promising cathode material.

As can be seen from the aforementioned studies, cobalt-based perovskite-related materials have the major drawback of higher TEC compared to the other SOFC components, along with the cost factor of cobalt, which has triggered research efforts for the development of cobalt-free materials over the past years. The most prominent materials of this category are presented in this section. Li et al. [104] examined the electrochemical performance of SrFe$_{0.7}$Cu$_{0.3}$O$_{3-\delta}$. The reported conductivities varied between 25 and 54 S/cm in the temperature range of 500–800 °C. Furthermore, the TEC curve studied over this temperature range has an average value close to the value of CGO electrolyte, mainly due to the significant decrease observed from Cu doping. Wu et al. [105] fabricated a copper-dopped SrFe$_{0.7}$Cu$_{0.3}$O$_{3-\delta}$ oxide (SFC) via solid state reaction. The average TEC of the developed cathode was approximate to the CGO electrolyte. At 700 °C, the lowest R$_p$ value of 0.14 Ωcm^2 in air was obtained revealing favorable electrochemical performance and good expectations for utilization as a cathode in IT-SOFCs.

In another study, Li et al. [106] investigated the cathode performance of GdBaFeNiO$_{5+d}$ fabricated via the EDTA-citrate complexing method on a Ce$_{0.8}$Sm$_{0.2}$O$_{1.9}$ (CSO) electrolyte. The authors reported that by impregnating a GdBaFeNiO$_{5+\delta}$ cathode with CSO nanoparticles a reduction in polarization resistance is achieved due to the enhanced ionic conductivity and the extension of the TPB zone of the cathode. The lowest R$_p$ was obtained at 700 °C, after three impregnations, equal to 0.065 Ωcm^2, a value that was approximately 14-times lower than that of the GdBaFeNiO$_{5+\delta}$ that was not impregnated. In general, the TEC values obtained were compatible with conventional electrolytes like CGO and CSO.

Yu et al. [107] examined SrFe$_{1-x}$Ti$_x$O$_{3-\delta}$ (x = 0–0.15) as an IT-SOFC cathode. The SFT material exhibited good chemical compatibility with SDC and LSGM electrolytes, and the SFT oxide with x = 0.05 demonstrated the best electrochemical performance with a peak power density of 475 mW/cm^2. In 2022, Wang et al. [108] prepared Sr$_2$Fe$_{1.5-x}$Zn$_x$Mo$_{0.5}$O$_{6-\delta}$ powders via the solution combustion method. The maximum conductivity of 27.3 S/cm was obtained for the sample with x = 0.05 at 450 °C, while the maximum power densities of 636 mW/cm^2 and 262 mW/cm^2 were observed at 800 °C and 700 °C, respectively, for the produced symmetrical cell with GDC electrolyte. These outputs were comparable to those recently reported for perovskite cathodes with conventional electrolyte-supported sign cells and show that SFZnM is a potential candidate for selection as a cathode material.

Ruddlesden–Popper (RP) phase materials that also show mixed conductivity can also be used as potential cathodes. Kim et al. [109] prepared three different RP- nickelate cathode materials via solid state reaction with the general formula of Ln$_2$NiO$_{4+\delta}$, (Ln = La, Nd, and Pr) which were mixed with YSZ electrolyte material in order to form three composite cathodes. From the fabricated symmetrical cells that were examined, the PNO-YSZ composite achieved the lowest ASR value of 0.64 Ωcm^2 at 800 °C, which was 41% and 16% lower from the ASR values of the LNO-YSZ and NNO-YSZ composites, respectively. The PNO-YSZ composite also exhibited the lowest activation barrier for ORRs when compared to the other two composites, making it the most promising candidate among the tested composites.

HEAs' and HEOs' enhanced stability and electrochemical performance have increased research for their applicability as cathode electrodes. Drabowa et al. [110] fabricated an La$_{0.2}$Pr$_{0.2}$Nd$_{0.2}$Sm$_{0.2}$Gd$_{0.2}$BaCo$_2$O$_{5+\delta}$, abbreviated as the (La, Pr, Nd, Sm, Gd)BaCo$_2$O$_{5+\delta}$ high-entropy double-perovskite cathode, and evaluated its electrochemical performance in an Ni-CGO/CGO/LSGM/(La, Pr, Nd, Sm, Gd)BaCo$_2$O$_{5+\delta}$ electrolyte-supported SOFC at 850 °C with 5 vol% H$_2$ fuel while the cathode was exposed to air. The HEO-cathode

exhibited a low polarization resistance of 0.0374 Ωcm^2 at 900 °C. The produced SOFC exhibited high electrochemical performance, validated by the maximum power density of 857 mW/cm^2 achieved at 850 °C. Furthermore, Liu et al. [111] prepared an La$_{0.2}$Pr$_{0.2}$Ba$_{0.2}$Sr$_{0.2}$ Ca$_{0.2}$Co$_2$O$_3$ high-entropy perovskite oxide with the EDTA-citrate method. At 700 °C, the low Rp value of 0.03 Ωcm^2 indicated enhanced catalytic performance. The performance of the Ln-BSC cathode was also evaluated in an anode-supported Ni-YSZ/YSZ-CGO/Ln-BSC at the same operating temperature with humidified hydrogen as the fuel and air as the oxidant. The obtained peak power density of 792 mW/cm^2 along with the cathode's enhanced tolerance to carbon dioxide demonstrated that the fabricated cathode is a promising material for IT-SOFCs.

In another study, Lu et al. [112] designed a Pr$_{0.5}$Ba$_{0.5}$Fe$_{0.2}$Co$_{0.2}$Ni$_{0.2}$Cu$_{0.2}$Mn$_{0.2}$O$_{3-d}$, abbreviated as HEPBM, high-entropy cathode via the combustion method. The performance of the new electrode was compared to that of the conventional PBM cathode in an SOFC with an SrFe$_{1.4}$Mg$_{0.1}$Mo$_{0.5}$O$_{6-\delta}$ anode and LSGM electrolyte at 850 °C and with wet H$_2$ fuel. The HEPBM electrode demonstrated a polarization resistance of 0.084 Ωcm^2 which was approximately 48% lower than the corresponding value for the PBM cathode (0.173 Ωcm^2) while the maximum power density obtained for the SOFC with the HEPBM cathode was 54.8% higher (962.39 mW/cm^2) compared to the SOFC with a PBM cathodic electrode. The obtained results revealed a significant enhancement of the electrochemical performance and stability of the fabricated cathode. Finally, Salman et al. [113] fabricated a high-entropy La$_{0.2}$Sr$_{0.2}$Pr$_{0.2}$Nd$_{0.2}$.Sm$_{0.2}$FeO$_{3-\delta}$ SrFe$_{1.4}$Mg$_{0.1}$Mo$_{0.5}$O$_{6-\delta}$ as an IT-SOFC cathode. The examined cell with an NiO-YSZ anode with YSZ electrolyte with a GDC buffer layer and the HE-LSF cathode exhibited polarization resistances of 0.21 Ωcm^2 and 0.101 Ωcm^2 at 700 °C and 800 °C, respectively, for wet H$_2$ (3% H$_2$O) as the anodic fuel and air as the oxidant. The corresponding peak power densities were 582 mW/cm^2 and 1029 mW/cm^2 for the aforementioned operating temperatures, proving that the designed high-entropy cathode can be utilized for IT-SOFCs.

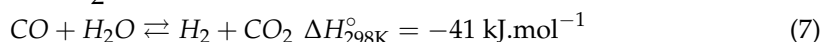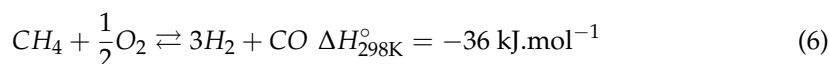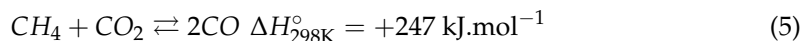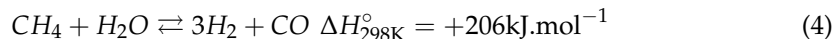## 3. Fuels Used in Solid Oxide Fuel Cells

Although the selection of electrode and electrolyte materials is vital to SOFC performance, another factor of major importance is also the type of fuel used in the anodic chamber [114]. Hydrogen is widely considered as the ideal fuel for SOFCs since it is electrochemically oxidized to produce water while emitting no greenhouse gases such as CO$_2$ or CO [115]. The higher heating value (HHV) of 141.9 MJ/kg for H$_2$ is the highest among other fossil fuels and has led researchers to increase its use in solid oxide fuel cell over the past decades as a clean fuel option. However, even though efforts to produce hydrogen from renewable sources have significantly progressed, and their share is continuing to increase, global hydrogen production continues to rely on fossil fuel feedstocks with a percentage of approximately 90% [116].

Also, the rigorous requirements that must be met for the transportation and storage of hydrogen along with the wide flammability range and the low ignition energy of H$_2$ have rendered this option quite risky and shifted the research attention on the operation of SOFCs with alternative fuels until, at least, the hydrogen value chain and its involved infrastructures become mature enough to overcome the involved problems. The use of alternative fuels in SOFCs has been extensively investigated by many elaborate reviews [19,21,117–119] that focus mainly on the associated problems of cell stability and degradation. In this section, the main fuel categories selected in practical SOFC systems (hydrocarbon fuels, solid carbon fuels, and alcohol fuels) will be briefly reported in terms of their applications in recent research attempts.
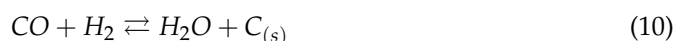
3.1. Hydrocarbon Fuels

Although the direct electrochemical oxidation of a fuel is the most effective way for its conversion, in the case of hydrocarbons, it is unlikely that this can take place in one single step, even for the simplest hydrocarbon such as CH$_4$. This is happening as the internal

reactions that occur at the fuel electrode are a combination of in situ anode reactions such as direct oxidation, reforming, and decomposition [120,121]. The main internal reforming processes include steam reforming (Equation (4)), dry reforming (Equation (5)), partial oxidation (Equation (6)), and water–gas shift reaction (Equation (7)).

$$CH_4 + H_2O \rightleftarrows 3H_2 + CO \ \Delta H^\circ_{298K} = +206 \text{kJ.mol}^{-1} \tag{4}$$

$$CH_4 + CO_2 \rightleftarrows 2CO \ \Delta H^\circ_{298K} = +247 \text{ kJ.mol}^{-1} \tag{5}$$

$$CH_4 + \frac{1}{2}O_2 \rightleftarrows 3H_2 + CO \ \Delta H^\circ_{298K} = -36 \text{ kJ.mol}^{-1} \tag{6}$$

$$CO + H_2O \rightleftarrows H_2 + CO_2 \ \Delta H^\circ_{298K} = -41 \text{ kJ.mol}^{-1} \tag{7}$$

Steam and dry reforming reactions are highly endothermic and convert methane or carbon dioxide into syngas while, at the same time, the water–gas shift reaction generates additional H_2. The main degradation problem that appears when hydrocarbons are fed as anode fuels is carbon deposition which takes place mainly due to hydrocarbon decomposition (Equation (8)), the Boudouard reaction (Equation (9)), and the reverse water–gas shift reaction (Equation (10)).

$$C_xH_y \longrightarrow \frac{x}{2}H_2 + yC_{(s)} \tag{8}$$

$$2CO \rightleftarrows CO_2 + C_{(s)} \tag{9}$$

$$CO + H_2 \rightleftarrows H_2O + C_{(s)} \tag{10}$$

Higher hydrocarbon fuels such as ethane (C_2H_6), propane (C_3H_8), and octane (C_8H_{18}) have characteristics like a liquid state and easier liquefaction properties in comparison to methane and can be effectively used for SOFC. Furthermore, the strength of the C-H bonds weaken with the increase in hydrocarbon chain length (CH_4: 435 kJ/mol; C_4H_{10}: 409 kJ/mol), and this promotes the conversion of higher hydrocarbon fuels to syngas through the reforming reactions [122]. Table 1 presents an overview of the most recent research efforts for hydrocarbon use in SOFCs with reference to the fuel mixture used, the configuration of the tested cells, and the maximum power density achieved.

Table 1. Hydrocarbon-fueled SOFCs and their electrochemical performance.

Fuel	Configuration: Anode/ Electrolyte/Cathode	Maximum Power Density (mW/cm²)	Ref.
CH_4–steam mixture (S/C = 2)	Cell with symmetric doubled-sided cathodes: Ni-YSZ/YSZ/GDC/LSCF	360 under 0.7 V at 850 °C	[123]
CH_4–steam mixture (S/C = 0.3)	Au-Ni-GDC/YSZ/LSM		[124]
Wet CH_4 (3% steam)	Anode-supported: $Ni_{0.875}Cu_{0.1}Mg_{0.025}$O-SDC/LSCF-SDC	670 at 700 °C	[125]
40 SCCM air- 80 SCCM CH_4	Ni-GDC/GCD/LSCF-GDC	1350 at 650 °C	[126]
CH_4	Anode-supported: CeO_2-Ni-GDC/GDC/GDC-BSCF	545 at 600 °C	[127]
Propane–air mixture (12% vol propane)	Ni-YSZ/YSZ/GDC/LSCF	670 at 700 °C	[128]
Propane	BaO deposited Ni-YSZ/YSZ/SDC/LSCF	880 at 750 °C	[129]
Wet octane (6.5% iso-octane, 3% steam)	Ni-YSZ-BZY/YSZ/LSCF	600 at 750 °C	[130]
Ethane	LST-Cr_2O_3/BXZY/GDC/LSCF-BCZY	320 at 750 °C	[131]

3.2. Alcohol Fuels

Liquid fuels have several advantages, including ease of transportation, storage, and distribution. Therefore, the utilization of alcohol fuels such as methanol and ethanol in SOFCs has been thoroughly investigated for many years. Alcohols, in contrast to higher hydrocarbons, exhibit reduced risk of coking since their carbon atoms are fewer, and their oxygen/carbon atom ratios are higher. Since methanol is generated mainly by the reforming of natural gas, it can be considered a carrier for syngas. Furthermore, the absence of a C-C bond in methanol helps it to decompose easily back into a H_2-rich gas mixture at the SOFC typical temperature range, especially since the conventional Ni-based anodes are found to catalytically promote the decomposition reaction (Equation (11)) [132].

$$CH_3OH \rightarrow CO + 2H_2 \tag{11}$$

Ethanol has attracted more research compared to methanol because globally the bio-fuel production capacity is strongly influenced by renewable bio-ethanol (ethanol produced from biomass sources). Table 2 lists some notable research works focusing on alcohol-fueled SOFCs.

Table 2. Alcohol-fueled SOFCs and their electrochemical performance.

Fuel	Configuration: Anode/ Electrolyte/Cathode	Maximum Power Density (mW/cm^2)	Ref.
Methanol	Anode-supported: Ni-SDC/SDC/SSC-SDC	698 at 650 °C	[133]
Methanol–steam mixture (S/C = 2)	Flat-tube cell with double-sided cathodes: Ni-YSZ/YSZ/GDC/LSCF-GDC	250 at 750 °C	[134]
Methanol	Pd-Ni/GDC/LSCF-SDC	9 at 450 °C	[135]
Ethanol	Pd/Ni-YSZ/YSZ/Pt	196 at 750 °C	[136]
Ethanol	Ir-GDC/Ni-YSZ/YSZ/GDC/LSCF	420 under 0.6 V at 850 °C	[137]
Ethanol–steam mixture (molar ratio 1:1)	Anode-supported: Ni-BZCY/SDC/BSCF	750 at 750 °C	[138]

3.3. Solid Carbon Fuels

Another category of fuels that has received extensive research over the last decade is solid carbon fuels that are mainly used in direct carbon solid oxide fuel cells (DC-SOFCs). These include activated carbon, biomass-based carbon (biochar), and coal. DC-SOFCs present a series of advantages such as higher electric efficiency and lower CO_2 emission per generated electricity unit. They also eliminate the need for storage infrastructures like tanks [139]. DC-SOFCs convert the chemical energy of the solid carbon fuels directly into electricity bypassing the need of gasification.

However, the limited contact between the carbon fuel and the TPB surface together with the sluggish reaction kinetics inhibit the performance of the DC-SOFCs and hinders their commercialization, at least at the moment. A solution that has been examined is the development of molten metal anodes and fuel mixtures of molten carbonates and solid carbon [140]. Another significant drawback of DC-SOFCs is ensuring the continuous supply of solid fuel. When using coal, an additional purification step is required in the condition that its content is rich in sulfur. Table 3 presents a brief overview of the state-of-the-art solid carbon fuel cells along with data regarding their configurations and their electrochemical performance in terms of maximum power density as these have been reported by the relative research.

Table 3. Solid carbon-fueled SOFCs and their electrochemical performance.

Fuel	Configuration: Anode/ Electrolyte/Cathode	Maximum Power Density (mW/cm^2)	Ref.
Activated carbon	LSFNb/SDC/ScSZ/LSM-ScSZ	302.8 at 850 °C	[141]
Activated carbon–carbonate mixture	YSTCu-GDC/LSGM/LSCF	366 at 800 °C	[142]
Raw brown coal	Ag-GDC/YSZ/Ag-GDC	211.4 at 850 °C	[143]
Fe-loaded walnut shell char	Ag-GDC/YSZ/Ag-GDC	205 at 800 °C	[144]

4. Study of Biogas-Assisted Electrolysis over an LSC Anode in an Oxygen-Conducting SOFEC

In line with the above-discussed progress, biogas-assisted electrolysis tests were conducted, at 800 °C, in a water-cooled Ni-YSZ/YSZ/GDC/LSC commercial cell (fuel cell materials), as seen in Figure 2. The cell consists of a 400 μm-thick anode with a 3 μm 8% YSZ electrolyte along with a 3 μm GDC barrier layer and a 12 μm LCS anode. As shown above, in Figure 2 the cell is attached to the one end of a YSZ tube (15 cm length, 20 mm outer diameter, and 16 mm internal diameter) using a quartz–porcelain enamel (PEMCO FL, 187/1). The YSZ tube was consequently enclosed in a 21 cm long quartz tube closed at its bottom end in order to form a double-chamber electrolysis cell reactor. In order to fit and seal the cell to the YSZ tube, a high-temperature sealing ceramic paste was used, and the entire cell unit was placed inside a high-temperature furnace.
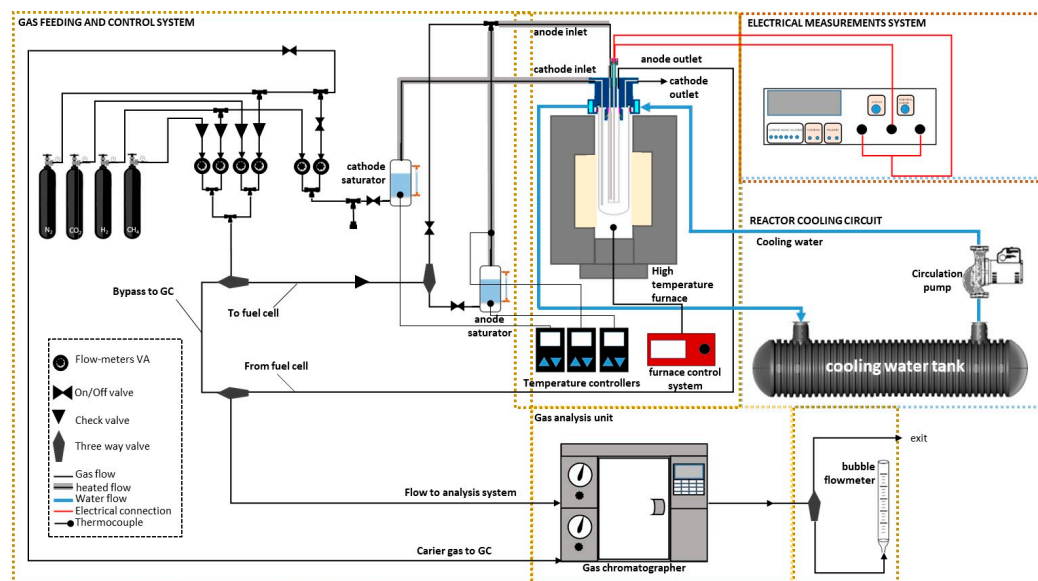
Figure 2. Schematic diagram of the experimental apparatus.

The unit is equipped with the proper gas feeding controls, product collection and analysis devices (GC equipped with a TCD detector), and an electricity collection and measurement system. Silver meshes, stuck to the electrodes with silver ink, were used for the current collection from both the anode and the cathode, while, for the electrical connections of the cell, gold wires were attached (using silver ink also) on these meshes on both the electrodes. Since, instead of the conventional Ni-YSZ, an LSC anode was used, 2% vol H$_2$ was added to the cathodic flow to prevent Ni oxidation at the cathode electrode.

A number of previous studies [145–154] have quoted the LSC electrode (either as an anode or as a cathode) in their work, which supports the selection of this anode material in this work, despite the detrimental phase reaction between LSC and YSZ that might take place. Previous studies [145–154] used LSC (raw and/or doped) as an anode in

SOFCs, thus advocating for the selection of LSC as an anode in this work. Moreover, Shen et al. [145] included LSC electrodes in their study that summarizes the research progress based on materials and discusses the merits and demerits of current cell materials in the electrochemical performance of RSOFCs. Kumar and Aruna [146], in their review paper, dedicated an extensive analysis on perovskite oxides such as LSC, LST, and LSV and their doped derivatives, and presented evidence from the literature for the suitability for SOFCs. This is particularly true for LSC doped with Ni and, moreover, Ru. Choolaei et al., in their review [147], studied several anode and cathode materials for each fuel cell technology, including Ni/GDC, LSC, LSCF, lithium metatitanate, porous Ni, and Pt.

Oh et al. [148] used LSC as both an anode and cathode (as LSC/K-MoSe$_2$) for water electrolysis, and found that the complementary charge transfer from LSC and K to MoSe$_2$ endows MoSe$_2$ with an electron-rich surface and increased electrical conductivity, which improves the hydrogen evolution reaction (HER) kinetics, and Thommy et al. [149] used an LSC anode with various dopants to achieve high-performance SOFCs. Thus, LSC composites have been found [148] to be robust and of excellent performance for the anodic oxygen evolution reaction.

Subotic and Hochenauer [150] and Raza et al. [151] provided encouraging information on the performance of LSC electrodes, while Zhao et al. [152] provided an input of La$_{0.6}$Sr$_{0.4}$CoO$_{3-\delta}$ (LSC)-impregnated porous SDC and GDC that has sustained encouraging and steady performance upon thermal cycling at temperature ranges from 500 to 800 °C for 30 days. In this line, Park and Hao [153] found that LSC has shown good performance in hydrocarbon fuels, and Petrov et al. [154] have found that the electrical conductivity of LSC materials is significantly higher than that of LSM, which is 3–10 times the electrical conductivity of LSM and shows higher catalytic activity when working in SOFC mode. Therefore, there are previous applications of LSC, raw or doped, as an electrode in SOFC, particularly with biogas as the fuel.

The above references do not mean that all possible problems related with the use of LSC electrodes have been resolved, but they support the statement that an LSC anode cannot be a priori rejected. In any case, the investigation of the stability of the materials used in SOFCs is not within the scope of this work, but it is part of another study that is in progress and will be presented in the near future.

In addition, it should be noted that the experimental results presented here are preliminary, mainly aiming to form a reference case for future experimentation, and, particularly, to initially evaluate the behavior of the materials used (anode, cathode, and electrolyte) in the cell structure. The stability of the materials used, a key issue for the long-term operation of the cell, is subject of another on-going work and will be presented in another paper in the near future.

4.1. Experimental Procedure

The first section of the experiments included operating the cell as an H$_2$-SOFC in order to determine the ASR and evaluate if the sealing was successful. A total of 100 cc·min^{-1} of 80% H$_2$ (mixture of 80 cc·min^{-1} pure H$_2$ and 20 cc·min^{-1} Argon) was fed to the NiO-YSZ electrode chamber in order to reduce nickel oxide, while the LSC chamber was fed with 100 cc·min^{-1} air. Figure 3 presents the I-V curve of the H$_2$-SOFC. For safety reasons, the measurements were taken up to −0.6 V due to the extremely reducing environment. The OCV was –1.225V, and for –0.6 V, the corresponding current density was 0.409 A/cm^2, resulting in an ASR of 1.52 Ωcm^2.

The next step was to evaluate the examined cell during methane-assisted electrolysis fuel cell (CH$_4$-SOFEC) operation before examining the biogas-assisted electrolysis. For the methane-assisted electrolysis experiments, the Ni-YSZ cathode was exposed to 100 cc·min^{-1} Ar with 60% v/v steam, and 2% v/v H$_2$ was added to prevent the oxidation of the Ni electrode. The biogas experiments were conducted with artificial CH$_4$/CO$_2$ mixtures of four different compositions, namely 80–20, 70–30, 60–40, and 50–50% for 100 cc·min^{-1} flow rates on both chambers and for 50 cc·min^{-1} anodic flow rate while the cathode flow

remained stable at 100 cc·min^{-1} in order to increase the reaction time at the anode and its effect on the performance of the cell. Analysis of the reactants and effluents was performed via an on-line Gas Chromatograph (Shimadzu 2014) equipped with Molecular Sieve 5A and Porapak Q columns. These analyses were taken at 1 V, 1.25 V, and 1.5 V along with the I–V curves.
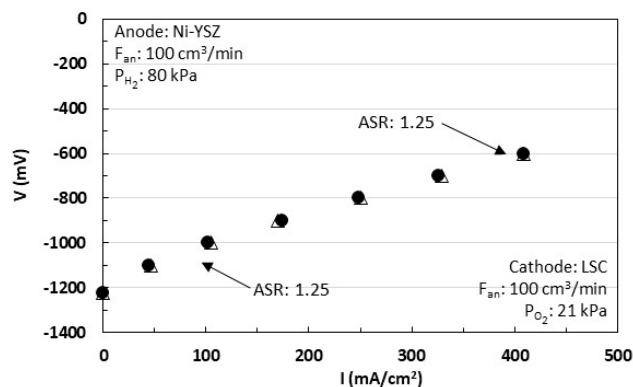

Figure 3. H_2-SOFC I−V curve at 800 °C.

4.2. Results

As mentioned above, the operation of the H_2-SOFC demonstrated a satisfying ASR value that enables the continuation of the experiments. For methane-assisted electrolysis, the maximum current at 1.5 V was reduced to 234 mA, as seen in Figure 4, resulting in an increased overall ASR of 3.41 Ωcm^2 which can be attributed to the lack of oxygen and the increase in the cell polarization.
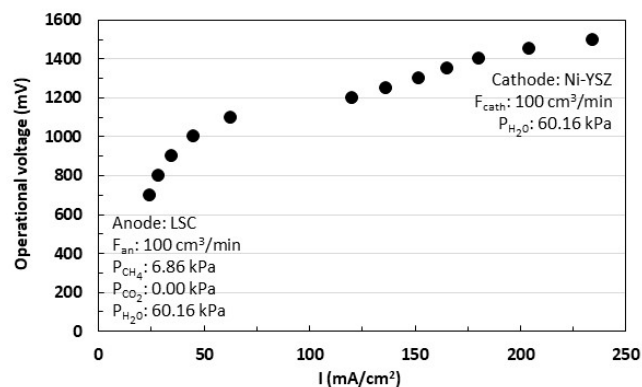
Figure 4. CH_4-SOFEC I-V curve at 800 °C.

Figures 5 and 6 presents the I-V curves for biogas-assisted electrolysis for the four different biogas compositions for the cases of anodic flow of 100 and 50 cc·min^{-1}, respectively.

For anodic and cathodic flow rates of 100 cc·min^{-1}, the current values slightly increased compared to the methane-SOFEC, and for the biogas mixture of equal content of methane and carbon dioxide, the corresponding value presented the higher increase of 11.6% (265 mA compared to 234 mA of the CH_4-SOFEC). The data from Figure 5 were used to calculate the apparent overall area specific resistances. The ASR calculated were doubled for the biogas-assisted electrolysis case ranging from 2.16 Ωcm^2 for the 50–50 biogas mixture up to 2.55 Ωcm^2 for the 80–20 biogas mixture.

Assuming that the remaining time of the reactants is not enough, the decrease of 50% in the anodic flow rate was examined, while the cathodic air supply remained stable. The data from Figure 6 demonstrated that the performance of the cell remained stable with a slight decrease in the current densities, with the exception of the 80–20 biogas case, where the current was reduced by approximately 41%. Regarding the chromatograph analyses,

the negative rates of carbon demonstrated that there is no carbon deposition, while in all the cases, CO was not traced in the effluents.

Using the data of Figures 7 and 8, the effect of the different biogas compositions in terms of maximum current density, ASR, and the methane conversion rate, respectively, were examined for the maximum flowrate. Under the anodic supply of steam, to prevent solid carbon deposition, the CO_2 content of biogas was found to increase the anodic CH_4 conversion and the obtained maximum current density, at the maximum applied potential at the SOFEC.
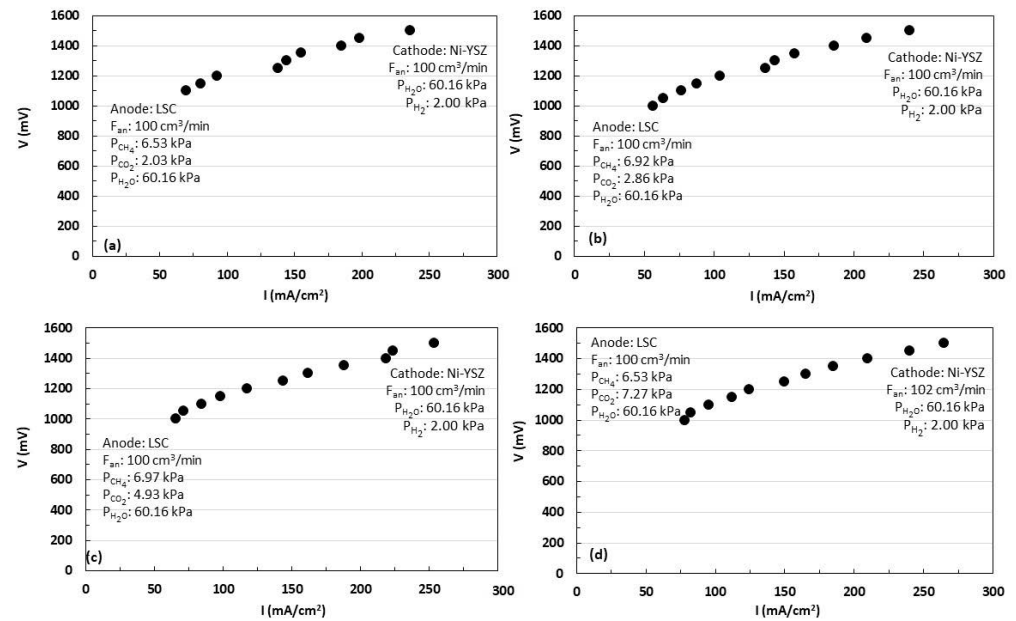
Figure 5. Biogas-assisted electrolysis I–V curves for biogas compositions of CH_4/CO_2 of (**a**) 80–20, (**b**) 70–30, (**c**) 60–40, and (**d**) 50–50 for 100 cc·min^{-1} flow rate at 800 °C.
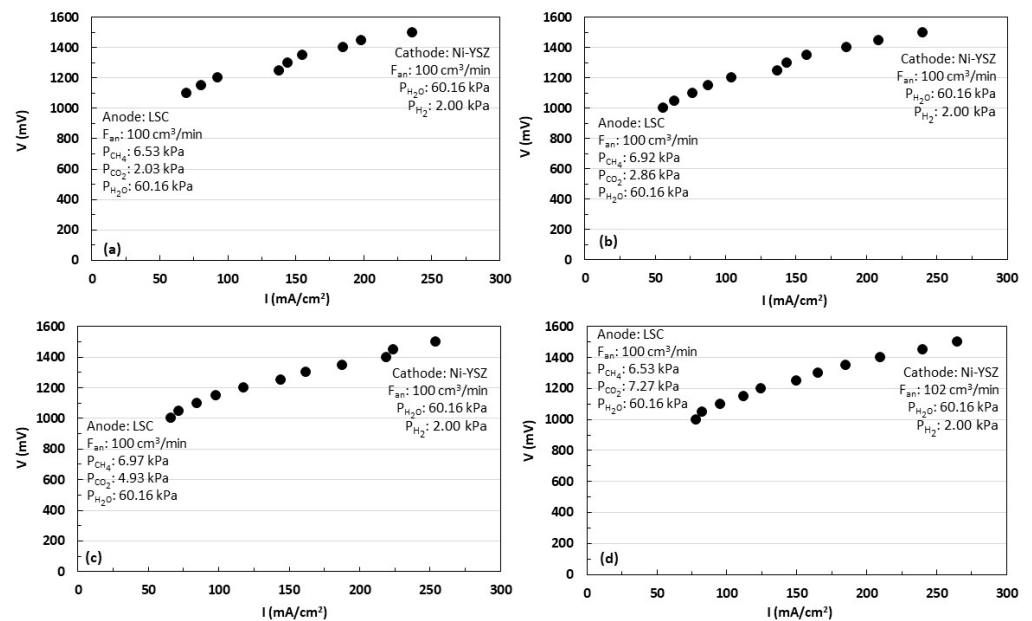
Figure 6. Biogas-assisted electrolysis I–V curves for biogas compositions of CH_4/CO_2 of (**a**) 80–20, (**b**) 70–30, (**c**) 60–40, and (**d**) 50–50 for 50 cc·min^{-1} flow rate at 800 °C.
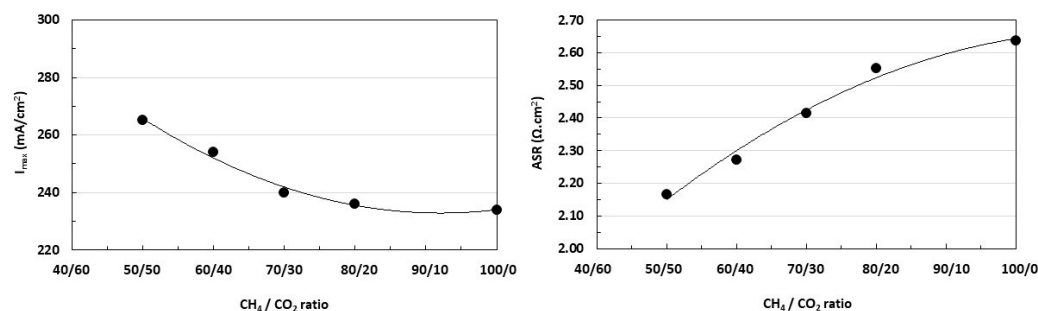
Figure 7. Maximum current and ASR curves for different biogas compositions of CH_4/CO_2 for 100 cc·min^{-1} flow rate at 800 °C.
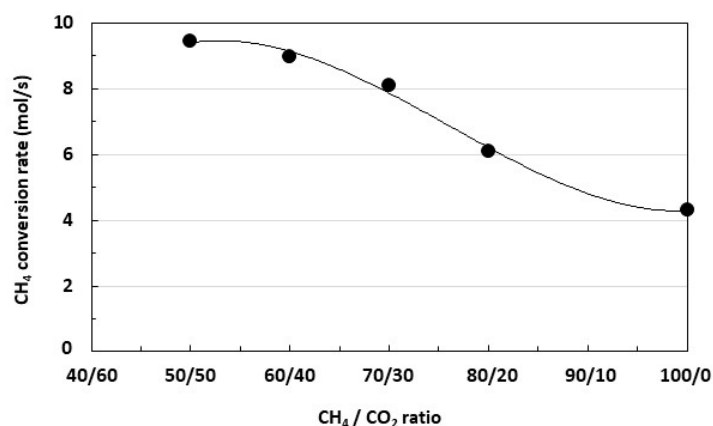

Figure 8. CH_4 conversion rated of the examined biogas compositions for 100 cc·min^{-1} flow rate at 800 °C.

In specific, under differential reaction conditions (CH_4 conversion below 10%), and for constant anodic CH_4 supply, by gradually decreasing the CH_4/CO_2 ratio from 1 (pure CH_4, for methane-assisted electrolysis) to 0.8, 0.7, 0.6, and 0.5 (corresponding to a biogas CH_4/CO_2 ratio of 80/20, 70/30, 60/40, and 50/50% v, and biogas-assisted operation) the obtained current density was found to increase from 234 to 236, 240, 254, and 265 mA·cm^{-2}, respectively. This corresponded to a 0.85, 2.56, 8.54, and 13.24% increase in cathodic H_2 production rate (from 1.21·10^{-6}, for methane, to 1.37·10^{-6} molH$_2$·s^{-1}·cm^{-2} for 50/50% CH_4/CO_2 biogas).

Overall, it was concluded that for constant anodic CH_4 supply, the increase in CO_2 led to increased CH_4 conversions at the anode, due to effect of the methane dry reforming (DMR) reaction and the sequential water–gas shift (WGS) reaction. This increased the anodic H_2 generation, which in turn decreased the anodic polarization of the SOFEC, resulting in increased current densities for the same operation potential.

For the examined differential conditions of the anodic CH_4 conversion, the specific electricity consumption for the cathodic H_2 generation at maximum operating potential was 289.45 kJ·mol H_2, corresponding to electric efficiencies in the range of 83.54%, based upon the generated H_2 HHV. Taking into account the anodic CH_4 combustion, the overall SOFEC efficiency for 1500 mV operating potential (i.e., the HHV of the generated H_2, over the combined electricity and CH_4 consumption) was found to be in the range of 40.78–57.25%.

5. Conclusions

This work focused on the ongoing research for the development of novel materials for anodes, cathodes, and oxygen-conducting solid electrolytes of SOFCs operating with hydrogen, hydrocarbons, alcohols, and solid carbon fuels. Recent advances have been presented by critically discussing many new reports for both electrocatalysts, scanning the

wide spectrum of available materials such as pure metals, metal alloys, cermets, perovskite oxides, and Ruddlesden–Popper phase materials. Scandia-stabilized-zirconia, perovskite oxides, and ceria-based solid electrolytes have also been reviewed in view of the most recent and promising experimental results throughout the scientific community. The appropriate material selection for these fundamental SOFC elements is of paramount importance as it can enhance the efficiency and life span of the SOFC systems and can accelerate their successful commercialization. Based on the recent advances on the SOFCs identified, an experimental study was conducted to illuminate the performance of an LSC anode in a biogas-fueled Ni-YSZ/YSZ/GDC/LSC commercial anode-supported SOFEC cell. Results obtained were quite encouraging for the application of LSC as an anode in actual SOFC and SOFEC systems. Thus, a satisfying ASR value was achieved for H_2-SOFC, and for biogas-assisted electrolysis, the current values were slightly increased, compared to the methane-SOFEC, and for equimolar methane and carbon dioxide biogas. The anodic supply of steam (to prevent carbon deposition) increased the anodic CH_4 conversion and resulted in the maximum current density at the maximum applied potential at the SOFC. Furthermore, for constant anodic CH_4, the increase in CO_2 led to increased CH_4 conversions at the anode, due to effect of the methane dry reforming (DMR) reaction and the sequential water–gas shift (WGS) reaction. The experimental campaign is continued for further investigation of the stability of the materials used in SOF and justification and illumination of the above and will be presented in another paper in the near future.

Abbreviations

ASR	Area Specific ohmic Resistance
BSCF	Barium Strontium Cobalt Ferrite
BSCFM	Barium Strontium Cobalt Ferrite doped with Molybdenum
BSCFZ	Barium Strontium Cobalt Ferrite doped with Zinc
BZCY	Barium Cerium Yttrium Zirconate
CCL	Current-Collecting Layer
CGO	Cerium Gadolinium Oxide
CHP	Combined Heat and Power
CSO	Ceria Samarium Oxide
DC-SOFC	Direct Carbon-assisted Solid Oxide Fuel Cell
DMR	Methane Dry Reforming Reaction
EDTA	Ethylene Diamine Tetra-acetic Acid
GDC	Gadolinium-Doped Ceria
HEA	High-Entropy Alloys
HEO	High-Entropy Oxides
HHV	Higher Heating Value
IT-SOFC	Intermediate-Temperature Solid Oxide Fuel Cell
Ln-BSC	Lanthanum Praseodymium Barium Strontium Calcium Cobaltate
LNO	Lanthanum Nickelate
LSC	Lanthanum Strontium Cobalt
LSCCNb	Lanthanum Strontium Cobaltite Doped with Copper and Niobium
LSCF	Lanthanum Strontium Cobalt Ferrite
LSCFR	Ruthenium-and-Cerium-Doped Lanthanum Strontium Ferrite
LSCNT	Nickel-and-Cerium-Doped Lanthanum Strontium Titanate
LSCrM	Lanthanum Strontium Chromium Manganese Perovskite

LSGM	Lanthanum Strontium Gadolinium Magnesia
LSM	Lanthanum Strontium-Doped Manganite
LST	Lanthanum Strontium Titanate
LSTF	Titanium-Substituted Lanthanum Strontium Ferrite
LSTN	Nickel-Doped Lanthanum Strontium Titanate
LSTR	Ruthenium-Doped Lanthanum Strontium Titanate
LT-SOFC	Low-Temperature Solid Oxide Fuel Cell
MIEC	Mixed Ionic–Electronic Conductivity
OCV	Open Circuit Voltage
ORR	Oxygen Reduction Semi-Reaction
PLD	Pulsed Laser Deposition
PNO	Praseodymium Nickelate
RP	Ruddlesden–Popper-Type Oxides
ScSZ	Scandia- Stabilized Zirconia
SCT	Strontium Tantalum Cobaltite
SDC	Samarium-Doped Ceria
SFC	Copper-Doped Strontium Ferrite
SFZnM	Strontium Ferrite Molybdate Doped with Zinc
SFT	Strontium Titanate Ferrite
SLT	Strontium Lanthanum Titanate
SMM	Strontium Manganese molybdate
SOFC	Solid Oxide Fuel Cell
SOFEC	Solid Oxide Fuel-Assisted Electrolysis Cell
SSZ	Scandia Stabilized Zirconia
SUS 430	Ferritic Stainless Steel Containing Max 18% Chromium
SVFMO	Strontium Vanadium Ferrite Molybdenum Oxide
TEC	Thermal Expansion Coefficient
TPB	Three Phase Boundary
VAN	Vertically Aligned Nano-Columns
WGS	Water–Gass Shift Reaction
YSZ	Yttria Stabilized Zirconia

References

1. Dawood, F.; Anda, M.; Shafiullah, G.M. Hydrogen Production for Energy: An Overview. *Int. J. Hydrogen Energy* **2020**, *45*, 3847–3869. [CrossRef]
2. Martins, F.; Felgueiras, C.; Smitkova, M.; Caetano, N. Analysis of Fossil Fuel Energy Consumption and Environmental Impacts in European Countries. *Energies* **2019**, *12*, 964. [CrossRef]
3. Jamal, T.; Shafiullah, G.M.; Dawood, F.; Kaur, A.; Arif, M.T.; Pugazhendhi, R.; Elavarasan, R.M.; Ahmed, S.F. Fuelling the future: An in-depth review of recent trends, challenges and opportunities of hydrogen fuel cell for a sustainable hydrogen economy. *Energy Rep.* **2023**, *10*, 2103–2127. [CrossRef]
4. Pramuanjaroenkij, A.; Kakac, S. The fuel cell electric vehicles: The highlight review. *Int. J. Hydrogen Energy* **2023**, *48*, 9401–9425. [CrossRef]
5. Waseem, M.; Amir, M.; Lakshmi, G.S.; Harivardhagini, S.; Ahmad, M. Fuel cell-based hybrid electric vehicles: An integrated review of current status, key challenges, recommended policies, and future prospects. *Green Energy Intell. Transp.* **2023**, *2*, 100121. [CrossRef]
6. Cigolotti, V.; Genovese, M.; Fragiacomo, P. Comprehensive review on fuel cell technology for stationary applications as sustainable and efficient poly-generation energy systems. *Energies* **2021**, *14*, 4963. [CrossRef]
7. Singh, M.; Zappa, D.; Comini, E. Solid oxide fuel cell: Decade of progress, future perspectives and challenges. *Int. J. Hydrogen Energy* **2021**, *46*, 27643–27674. [CrossRef]
8. Jang, I.; Carneiro, J.S.A.; Crawford, J.O.; Cho, Y.J.; Parvin, S.; Gonzalez-Casamachin, D.A.; Baltrusaitis, J.; Lively, R.P.; Nikolla, E. Electrocatalysis in Solid Oxide Fuel Cells and electrolyzers. *Chem. Rev.* **2024**, *124*, 8233–8306. [CrossRef]
9. Wang, Y.; Shi, J.; Gu, X.; Deutschmann, O.; Shi, Y.; Cai, N. Toward mobility of solid oxide fuel cells. *Progress. Energy Combust. Sci.* **2024**, *102*, 101141. [CrossRef]
10. Arshad, M.S.; Mbianda, X.Y.; Ali, I.; Wanbing, G.; Kamal, T.; Kauhaniemi, K.; Hassan, A.Z.; Ghulam, Y. Advances and perspectives on Solid Oxide Fuel Cells: From nanotechnology to power electronic devices. *Energy Technol.* **2023**, *11*, 2300452. [CrossRef]
11. Talukdar, A.; Chakrovorty, A.; Sarmah, P.; Paramasivam, P.; Kumar, V.; Yadav, S.K.; Manickkam, S. A review on Solid Oxide Fuel Cell technology: An efficient energy conversion system. *Int. J. Energy Res.* **2024**, *6443247*, 1–20. [CrossRef]
12. Scott, K. Introduction to Hydrogen, Electrolyzers and Fuel Cells Science and Technology. *Compr. Renew. Energy* **2022**, *4*, 1–28. [CrossRef]

13. Stambouli, A.B.; Traversa, E.; Stambouli, A. Solid. Oxide Fuel Cells (SOFCs): A Review of an Environmentally Clean and Efficient Source of Energy. *Renew. Sustain. Energy Rev.* **2002**, *6*, 433–455. [CrossRef]

14. Larminie, J.; Dicks, A. *Fuel Cell Systems Explained*; John Wiley: Hoboken, NJ, USA, 2003.

15. Singhal, S.C. Solid Oxide Fuel Cells for Power Generation. *Wiley Interdiscip. Rev. Energy Environ.* **2014**, *3*, 179–194. [CrossRef]

16. Shu, L.; Sunarso, J.; Hashim, S.S.; Mao, J.; Zhou, W.; Liang, F. Advanced Perovskite Anodes for Solid Oxide Fuel Cells: A Review. *Int. J. Hydrogen Energy* **2019**, *44*, 31275–31304. [CrossRef]

17. Hanna, J.; Lee, W.Y.; Shi, Y.; Ghoniem, A.F. Fundamentals of electro- and thermochemistry in the anode of solid-oxide fuel cells with hydrocarbon and syngas fuels. *Prog. Energy Combust. Sci.* **2014**, *40*, 74–111. [CrossRef]

18. Abdalla, A.M.; Hossain, S.; Nisfindy, O.B.; Azad, A.T.; Dawood, M.; Azad, A.K. Hydrogen Production, Storage, Transportation and Key Challenges with Applications: A Review. *Energy Convers. Manag.* **2018**, *165*, 602–627. [CrossRef]

19. Yu, F.; Han, T.; Wang, Z.; Xie, Y.; Wu, Y.; Jin, Y.; Yang, N.; Xiao, J.; Kawi, S. Recent Progress in Direct Carbon Solid Oxide Fuel Cell: Advanced Anode Catalysts, Diversified Carbon Fuels, and Heat Management. *Int. J. Hydrogen Energy* **2021**, *46*, 4283–4300. [CrossRef]

20. McIntosh, S.; Gorte, R.J. Direct Hydrocarbon Solid Oxide Fuel Cells. *Chem. Rev.* **2004**, *104*, 4845–4865. [CrossRef]

21. Wang, W.; Su, C.; Wu, Y.; Ran, R.; Shao, Z. Progress in Solid Oxide Fuel Cells with Nickel-Based Anodes Operating on Methane and Related Fuels. *Chem. Rev.* **2013**, *113*, 8104–8151. [CrossRef]

22. Dwivedi, S. Solid oxide fuel cell: Materials for anode, cathode and electrolyte. *Int. J. Hydrogen Energy* **2020**, *45*, 23988–24013. [CrossRef]

23. Yatoo, M.A.; Habib, F.; Malik, A.H.; Mohsin, J.Q.; Ahmad, S.; Ganayee, M.A.; Ahmad, Z. Solid-oxide fuel cells: A critical review of materials for cell components. *MRS Commun.* **2023**, *13*, 378–384. [CrossRef]

24. Hussain, S.; Yangping, L. Review of solid oxide fuel cell materials: Cathode, anode, and electrolyte. *Energy Transit.* **2020**, *4*, 113–126. [CrossRef]

25. Vinchhi, P.; Khandla, M.; Chaudhary, K.; Pati, R. Recent advances on electrolyte materials for SOFC: A review. *Inorg. Chem. Commun.* **2023**, *152*, 110724. [CrossRef]

26. Scott, H.G. Phase Relationships in the Zirconia-Yttria System. *J. Mater. Sci.* **1975**, *10*, 1527–1535. [CrossRef]

27. Wang, F.; Lyu, Y.; Chu, D.; Jin, Z.; Zhang, G.; Wang, D. The Electrolyte Materials for SOFCs of Low-Intermediate Temperature: Review. *Mater. Sci. Technol.* **2019**, *35*, 1551–1562. [CrossRef]

28. Arachi, Y.; Sakai, H.; Yamamoto, O.; Takeda, Y.; Imanishai, N. Electrical conductivity of the ZrO_2–Ln_2O_3 (Ln=lanthanides) system. *Solid State Ion.* **1999**, *121*, 133–139. [CrossRef]

29. Yamamoto, O.; Arachi, Y.; Sakai, H.; Takeda, Y.; Imanishi, N.; Mizutani, Y.; Kawai, M.; Nakamura, Y. Zirconia Based Oxide Ion Conductors for Solid Oxide Fuel Cells. *Ionics* **1998**, *4*, 403–408. [CrossRef]

30. Ju, H.K.; Badwal, S.; Giddey, S. A Comprehensive Review of Carbon and Hydrocarbon Assisted Water Electrolysis for Hydrogen Production. *Appl. Energy* **2018**, *231*, 502–533. [CrossRef]

31. Hanif, M.B.; Rauf, S.; Motola, M.; Babar, Z.U.D.; Li, C.-J. Recent progress of perovskite-based electrolyte materials for solid oxide fuel cells and performance optimizing strategies for energy storage applications. *Mater. Res. Bull.* **2022**, *146*, 111612. [CrossRef]

32. Helal, H.; Ahrouch, M.; Rabehi, A.; Zappa, D.; Comini, E. Nanostructured materials for enhanced performance of Solid Oxide Fuel Cells: A comprehensive review. *Crystals* **2024**, *14*, 306. [CrossRef]

33. Baratov, S.; Filonova, E.; Ivanova, A.; Hanif, A.B.; Irshad, M.; Khan, M.Z.; Motola, M.; Rauf, S.; Medvedev, D. Current and further trajectories in designing functional materials for solid oxide electrochemical cells: A review of other reviews. *J. Energy Chem.* **2024**, *94*, 302–331. [CrossRef]

34. Voorhoeve, R.J.H. Perovskite-Related Oxides as Oxidation—Reduction Catalysts. *Adv. Mater. Catal.* **1977**, *195*, 129–180. [CrossRef]

35. Ishihara, T.; Matsuda, H.; Takita, Y. Doped LaGaOg Perovskite Type Oxide as a New Oxide Ionic Conductor. *J. Am. Chem. Soc.* **1994**, *116*, 3801–3803. [CrossRef]

36. Ishihara, T.; Matsuda, H.; Takita, Y. Effects of Rare Earth Cations Doped for La Site on the Oxide Ionic Conductivity of LaGaO,-Based Perovskite Type Oxide. *Solid State Ion.* **1995**, *79*, 147–151. [CrossRef]

37. Huang, K.; Tichy, R.S.; Goodenough, J.B. Superior Perovskite Oxide-Ion Conductor; Strontium-and Magnesium-Doped $LaGaO_3$: I, Phase Relationships and Electrical Properties. *J. Am. Ceram. Soc.* **1998**, *81*, 2565–2575. [CrossRef]

38. Zhang, J.; Lenser, C.; Menzler, N.H.; Guillon, O. Comparison of Solid Oxide Fuel Cell (SOFC) Electrolyte Materials for Operation at 500 °C. *Solid. State Ion.* **2020**, *344*, 115138. [CrossRef]

39. Hwang, C.S.; Hwang, T.J.; Tsai, C.H.; Chang, C.L.; Yang, S.F.; Wu, M.H.; Fu, C.Y. Effect of Plasma Spraying Power on LSGM Electrolyte of Metal-Supported Solid Oxide Fuel Cells. *Ceram. Int.* **2017**, *43*, S591–S597. [CrossRef]

40. Wang, L.S.; Li, C.X.; Li, G.R.; Yang, G.J.; Zhang, S.L.; Li, C.J. Enhanced Sintering Behavior of LSGM Electrolyte and Its Performance for Solid Oxide Fuel Cells Deposited by Vacuum Cold Spray. *J. Eur. Ceram. Soc.* **2017**, *37*, 4751–4761. [CrossRef]

41. Kim, K.J.; Choi, S.W.; Kim, M.Y.; Lee, M.S.; Kim, Y.S.; Kim, H.S. Fabrication Characteristics of SOFC Single Cell with Thin LSGM Electrolyte via Tape-Casting and Co-Sintering. *J. Ind. Eng. Chem.* **2016**, *42*, 69–74. [CrossRef]

42. Inaba, H.; Tagawa, H. Ceria-Based Solid Electrolytes. *Solid State Ion.* **1996**, *83*, 1–6. [CrossRef]

43. Kim, G.; Lee, N.; Kim, K.B.; Kim, B.K.; Chang, H.; Song, S.J.; Park, J.Y. Various Synthesis Methods of Aliovalent-Doped Ceria and Their Electrical Properties for Intermediate Temperature Solid Oxide Electrolytes. *Int. J. Hydrogen Energy* **2013**, *38*, 1571–1587. [CrossRef]

44. Steele, B.C.H. Appraisal of $Ce_{1-y}Gd_yO_{2-y/2}$ Electrolytes for IT-SOFC Operation at 500 °C. *Solid. State Ion.* **2000**, *129*, 95–110. [CrossRef]

45. Atkinson, A. Solid Oxide Fuel Cell Electrolytes-Factors Influencing Lifetime. In *Solid Oxide Fuel Cell Lifetime and Reliability: Critical Challenges in Fuel Cells*; Academic Press: Cambridge, MA, USA, 2017; pp. 19–35. [CrossRef]

46. Zhang, X.; Robertson, M.; Deĉes-Petit, C.; Qu, W.; Kesler, O.; Maric, R.; Ghosh, D. Internal Shorting and Fuel Loss of a Low Temperature Solid Oxide Fuel Cell with SDC Electrolyte. *J. Power Sources* **2007**, *164*, 668–677. [CrossRef]

47. Ahmed, N.; Devi, S.; Dar, M.A.; Ibrahim, S.K.M.; Sharma, A.; Sharma, N.; Paul, S.; Ahamed, S.R. Anode material for solid oxide fuel cell: A review. *Indian J. Phys.* **2024**, *98*, 877–888. [CrossRef]

48. Liu, W.; Flytzani-stephanopoulos, M. Total Oxidation of Carbon Monoxide and Methane over Transition Metal Fluorite Oxide Composite Catalysts: I. Catalyst Composition and Activity. *J. Catal.* **1995**, *153*, 304–316. [CrossRef]

49. Khan, M.S.; Lee, S.B.; Song, R.H.; Lee, J.W.; Lim, T.H.; Park, S.J. Fundamental Mechanisms Involved in the Degradation of Nickel–Yttria Stabilized Zirconia (Ni–YSZ) Anode during Solid Oxide Fuel Cells Operation: A Review. *Ceram. Int.* **2016**, *42*, 35–48. [CrossRef]

50. Simwonis, D.; Tietz, F.; Stöver, D. Nickel Coarsening in Annealed Ni/8YSZ Anode Substrates for Solid Oxide Fuel Cells. *Solid. State Ion.* **2000**, *132*, 241–251. [CrossRef]

51. Gorte, R.J.; Vohs, J.M.; McIntosh, S. Recent Developments on Anodes for Direct Fuel Utilization in SOFC. *Solid. State Ion.* **2004**, *175*, 1–6. [CrossRef]

52. Kim, H.; Vohs, J.M.; Gorte, R.J. Direct Oxidation of Sulfur-Containing Fuels in a Solid Oxide Fuel Cell. *Chem. Commun.* **2001**, *22*, 2334–2335. [CrossRef]

53. Lu, C.; Worrell, W.L.; Vohs, J.M.; Gorte, R.J. A Comparison of Cu-Ceria-SDC and Au-Ceria-SDC Composites for SOFC Anodes. *J. Electrochem. Soc.* **2003**, *150*, A1357. [CrossRef]

54. Kim, H.; Lu, C.; Worrell, W.L.; Vohs, J.M.; Gorte, R.J. Cu-Ni Cermet Anodes for Direct Oxidation of Methane in Solid-Oxide Fuel Cells. *J. Electrochem. Soc.* **2002**, *149*, A247. [CrossRef]

55. Costa-Nunes, O.; Gorte, R.J.; Vohs, J.M. Comparison of the Performance of Cu-CeO_2-YSZ and Ni-YSZ Composite SOFC Anodes with H2, CO, and Syngas. *J. Power Sources* **2005**, *141*, 241–249. [CrossRef]

56. Wang, Z.; Wang, Y.; Qin, D.; Gu, Y.; Yu, H.; Tao, S.; Qian, B.; Chao, Y. Improving Electrochemical Performance of (Cu, Sm)CeO_2 Anode with Anchored Cu Nanoparticles for Direct Utilization of Natural Gas in Solid Oxide Fuel Cells. *J. Eur. Ceram. Soc.* **2022**, *42*, 3254–3263. [CrossRef]

57. Tao, S.; Irvine, J.T.S. A Redox-Stable Efficient Anode for Solid-Oxide Fuel Cells. *Nat. Mater.* **2003**, *2*, 320–323. [CrossRef]

58. Zhu, X.; Lü, Z.; Wei, B.; Chen, K.; Liu, M.; Huang, X.; Su, W. Enhanced Performance of Solid Oxide Fuel Cells with Ni/CeO_2 Modified $La_{0.75}Sr_{0.25}Cr_{0.5}Mn_{0.5}O_{3-\delta}$ Anodes. *J. Power Sources* **2009**, *190*, 326–330. [CrossRef]

59. Jung, I.; Lee, D.; Lee, S.O.; Kim, D.; Kim, J.; Hyun, S.H.; Moon, J. LSCM-YSZ Nanocomposites for a High Performance SOFC Anode. *Ceram. Int.* **2013**, *39*, 9753–9758. [CrossRef]

60. Tao, S.; Irvine, J.T.S. Catalytic Properties of the Perovskite Oxide $La_{0.75}Sr_{0.25}Cr_{0.5}Fe_{0.5}O_{3-\delta}$ in Relation to Its Potential as a Solid Oxide Fuel Cell Anode Material. *Chem. Mater.* **2004**, *16*, 4116–4121. [CrossRef]

61. Fowler, D.E.; Haag, J.M.; Boland, C.; Bierschenk, D.M.; Barnett, S.A.; Poeppelmeier, K.R. Stable, Low Polarization Resistance Solid Oxide Fuel Cell Anodes: $La_{1-x}Sr_xCr_{1-x}Fe_xO_{3-\delta}$ (x = 0.2–0.67). *Chem. Mater.* **2014**, *26*, 3113–3120. [CrossRef]

62. Aliotta, C.; Liotta, L.F.; Deganello, F.; la Parola, V.; Martorana, A. Direct Methane Oxidation on $La_{1-x}Sr_xCr_{1-y}Fe_yO_{3-\delta}$ Perovskite-Type Oxides as Potential Anode for Intermediate Temperature Solid Oxide Fuel Cells. *Appl. Catal. B* **2016**, *180*, 424–433. [CrossRef]

63. Sun, Y.F.; Li, J.H.; Chuang, K.T.; Luo, J.L. Electrochemical Performance and Carbon Deposition Resistance of Ce-Doped $La_{0.7}Sr_{0.3}Fe_{0.5}Cr_{0.5}O_{3-\delta}$ Anode Materials for Solid Oxide Fuel Cells Fed with Syngas. *J. Power Sources* **2015**, *274*, 483–487. [CrossRef]

64. Sun, Y.; Li, J.; Zeng, Y.; Amirkhiz, B.S.; Wang, M.; Behnamian, Y.; Luo, J. A-Site Deficient Perovskite: The Parent for in Situ Exsolution of Highly Active, Regenerable Nano-Particles as SOFC Anodes. *J. Mater. Chem. A Mater.* **2015**, *3*, 11048–11056. [CrossRef]

65. Fowler, D.E.; Messner, A.C.; Miller, E.C.; Slone, B.W.; Barnett, S.A.; Poeppelmeier, K.R. Decreasing the Polarization Resistance of (La,Sr)$CrO_{3-\delta}$ Solid Oxide Fuel Cell Anodes by Combined Fe and Ru Substitution. *Chem. Mater.* **2015**, *27*, 3683–3693. [CrossRef]

66. Wang, J.; Fu, L.; Yang, J.; Wu, K.; Zhou, J.; Wu, K. Cerium and Ruthenium Co-Doped $La_{0.7}Sr_{0.3}FeO_{3-\delta}$ as a High-Efficiency Electrode for Symmetrical Solid Oxide Fuel Cell. *J. Rare Earths* **2021**, *39*, 1095–1099. [CrossRef]

67. Peng, X.; Tian, Y.; Liu, Y.; Wang, W.; Chen, J.; Li, J.; Chi, B.; Pu, J.; Li, J. A Double Perovskite Decorated Carbon-Tolerant Redox Electrode for Symmetrical SOFC. *Int. J. Hydrogen Energy* **2020**, *45*, 14461–14469. [CrossRef]

68. Zhao, H.; Gao, F.; Li, X.; Zhang, C.; Zhao, Y. Electrical Properties of Yttrium Doped Strontium Titanate with A-Site Deficiency as Potential Anode Materials for Solid Oxide Fuel Cells. *Solid. State Ion.* **2009**, *180*, 193–197. [CrossRef]

69. Park, B.H.; Choi, G.M. Ex-Solution of Ni Nanoparticles in a $La_{0.2}Sr_{0.8}Ti_{1-x}Ni_xO_{3-\delta}$ Alternative Anode for Solid Oxide Fuel Cell. *Solid. State Ion.* **2014**, *262*, 345–348. [CrossRef]

70. Sun, Y.F.; Zhou, X.W.; Zeng, Y.; Amirkhiz, B.S.; Wang, M.N.; Zhang, L.Z.; Hua, B.; Li, J.; Li, J.H.; Luo, J.L. An Ingenious Ni/Ce Co-Doped Titanate Based Perovskite as a Coking-Tolerant Anode Material for Direct Hydrocarbon Solid Oxide Fuel Cells. *J. Mater. Chem. A Mater.* **2015**, *3*, 22830–22838. [CrossRef]

71. Yoon, H.; Zou, J.; Sammes, N.M.; Chung, J. Ru-Doped Lanthanum Strontium Titanates for the Anode of Solid Oxide Fuel Cells. *Int. J. Hydrogen Energy* **2015**, *40*, 10985–10993. [CrossRef]

72. Xu, J.; Zhou, X.; Dong, X.; Pan, L.; Sun, K. Catalytic Activity of Infiltrated $La_{0.3}Sr_{0.7}Ti_{0.3}Fe_{0.7}O_{3-\delta}$–$CeO_2$ as a Composite SOFC Anode Material for H2 and CO Oxidation. *Int. J. Hydrogen Energy* **2017**, *42*, 15632–15640. [CrossRef]

73. Sayagués, M.J.; Gotor, F.J.; Pueyo, M.; Poyato, R.; Garcia-Garcia, F.J. Mechanosynthesis of $Sr_{1-x}La_xTiO_3$ Anodes for SOFCs: Structure and Electrical Conductivity. *J. Alloys Compd.* **2018**, *763*, 679–686. [CrossRef]

74. Cao, Z.; Fan, L.; Zhang, G.; Shao, K.; He, C.; Zhang, Q.; Lv, Z.; Zhu, B. Titanium-Substituted Ferrite Perovskite: An Excellent Sulfur and Coking Tolerant Anode Catalyst for SOFCs. *Catal. Today* **2019**, *330*, 217–221. [CrossRef]

75. Huang, K.H.; Yeh, J.W. A Study on the Multicomponent Alloy Systems Containing Equal-Mole Elements. Master's Thesis, National Tsing Hua University, Hsinchu, Taiwan, 1996.

76. Yeh, J.W.; Chen, S.K.; Lin, S.J.; Gan, J.Y.; Chin, T.S.; Shun, T.T.; Tsau, C.H.; Chang, S.Y. Nanostructured High-Entropy Alloys with Multiple Principal Elements: Novel Alloy Design Concepts and Outcomes. *Adv. Eng. Mater.* **2004**, *6*, 299–303. [CrossRef]

77. Ma, G.; Chen, D.; Ji, S.; Bai, X.; Wang, X.; Huan, Y.; Dong, D.; Hu, X.; Wei, T. Medium-Entropy $SrV_{1/3}Fe_{1/3}Mo_{1/3}O_3$ with High Conductivity and Strong Stability as SOFCs High-Performance Anode. *Materials* **2022**, *15*, 2298. [CrossRef] [PubMed]

78. Lee, K.X.; Hu, B.; Dubey, P.K.; Anisur, M.R.; Belko, S.; Aphale, A.N.; Singh, P. High-Entropy Alloy Anode for Direct Internal Steam Reforming of Methane in SOFC. *Int. J. Hydrogen Energy* **2022**, *47*, 38372–38385. [CrossRef]

79. Yamamoto, O. Solid Oxide Fuel Cells: Fundamental Aspects and Prospects. *Electrochim. Acta* **2000**, *45*, 2423–2435. [CrossRef]

80. Sun, C.; Hui, R.; Roller, J. Cathode Materials for Solid Oxide Fuel Cells: A Review. *J. Solid. State Electrochem.* **2010**, *14*, 1125–1144. [CrossRef]

81. He, S.; Zou, Y.; Chen, K.; Jiang, S.P. A critical review of key materials and issues in solid oxide cells. *Interdiscip. Mater.* **2023**, *2*, 111–136. [CrossRef]

82. Brett, D.J.L.; Atkinson, A.; Brandon, N.P.; Skinner, S.J. Intermediate Temperature Solid Oxide Fuel Cells. *Chem. Soc. Rev.* **2008**, *37*, 1568–1578. [CrossRef]

83. Murray, E.P.; Tsai, T.; Barnett, S.A. Oxygen transfer processes in (La, Sr) MnO_3/Y_2O_3-stabilized ZrO_2 cathodes: An impedance spectroscopy study. *Solid State Ion.* **1998**, *110*, 235–243. [CrossRef]

84. Ji, Y.; Kilner, J.A.; Carolan, M.F. Electrical Properties and Oxygen Diffusion in Yttria-Stabilised Zirconia (YSZ)-$La_{0.8}Sr_{0.2}MnO_{3\pm\delta}$ (LSM) Composites. *Solid. State Ion.* **2005**, *176*, 937–943. [CrossRef]

85. Park, J.; Zou, J.; Chung, J. Synthesis and Evaluation of Nano-Size Lanthanum Strontium Manganite-Yttria-Stablized Zirconia Composite Powders as Cathodes for Solid Oxide Fuel Cells. *J. Power Sources* **2010**, *195*, 4593–4599. [CrossRef]

86. Su, Q.; Yoon, D.; Sisman, Z.; Khatkhatay, F.; Jia, Q.; Manthiram, A.; Wang, H. Vertically Aligned Nanocomposite $La_{0.8}Sr_{0.2}MnO_{3-\delta}/Zr_{0.92}Y_{0.08}O_{1.96}$ Thin Films as Electrode/Electrolyte Interfacial Layer for Solid Oxide Reversible Fuel Cells. *Int. J. Hydrogen Energy* **2013**, *38*, 16320–16327. [CrossRef]

87. Wang, A.; Wang, X.; Qiu, P.; Yang, J.; Yang, X.; Hua, S.; Chi, B.; Pu, J.; Li, J. Performance and Durability of an Anode-Supported Solid Oxide Fuel Cell with a PdO/ZrO_2 Engineered $(La_{0.8}Sr_{0.2})_{0.95}MnO_3$-Δ-$(Y_2O_3)_{0.08}(ZrO_2)_{0.92}$ Composite Cathode. *Int. J. Hydrogen Energy* **2018**, *43*, 12368–12376. [CrossRef]

88. Wang, G.; Wu, W.; Guan, W.; Jin, L.; Guo Wang, W. Effect of Conductivity and Adhesive Properties of Cathode Current-Collecting Layer on Cell Performance inside Stack for Planar Solid Oxide Fuel Cells. *Ceram. Int.* **2014**, *40*, 11023–11030. [CrossRef]

89. Park, J.-H.; Hong, W.-S.; Yoon, K.J.; Lee, J.-H.; Lee, H.-W.; Son, J.-W. Physical and Electrochemical Characteristics of Pulsed Laser Deposited $La_{0.6}Sr_{0.4}CoO_{3-\delta}$-$Ce_{0.9}Gd_{0.1}O_{2-\delta}$ Nanocomposites as a Function of the Mixing Ratio. *J. Electrochem. Soc.* **2014**, *161*, F16–F22. [CrossRef]

90. Tao, Y.; Shao, J.; Wang, J.; Wang, W.G. Synthesis and Properties of $La_{0.6}Sr_{0.4}CoO_{3-\delta}$ Nanopowder. *J. Power Sources* **2008**, *185*, 609–614. [CrossRef]

91. Wu, Y.C.; Huang, P.Y.; Xu, G. Properties and Microstructural Analysis of $La_{1-x}Sr_xCoO_{3-\delta}$ (X = 0–0.6) Cathode Materials. *Ceram. Int.* **2017**, *43*, 2460–2470. [CrossRef]

92. Son, J.-W.; Myung, D.-H.; Hwang, J.; Lee, H.-W.; Lee, J.-H. Potential and Limitation of Application of Pulsed Laser Deposited Nano-Structure LSC Thin Film Cathode to YSZ Electrolyte SOFC. *ECS Trans.* **2019**, *35*, 2423–2427. [CrossRef]

93. Chen, K.; Li, N.; Ai, N.; Cheng, Y.; Rickard, W.D.A.; Jiang, S.P. Polarization-Induced Interface and Sr Segregation of in Situ Assembled $La_{0.6}Sr_{0.4}Co_{0.2}Fe_{0.8}O_{3-\delta}$ Electrodes on Y_2O_3-ZrO_2 Electrolyte of Solid Oxide Fuel Cells. *ACS Appl. Mater. Interfaces* **2016**, *8*, 31729–31737. [CrossRef]

94. Murray, E.P.; Sever, M.J.; Barnett, S.A. Electrochemical Performance of $(La,Sr)(Co,Fe)O_3$-$(Ce,Gd)O_3$ Composite Cathodes. *Solid State Ion.* **2002**, *148*, 27–34. [CrossRef]

95. Lou, X.; Wang, S.; Liu, Z.; Yang, L.; Liu, M. Improving $La_{0.6}Sr_{0.4}Co_{0.2}Fe_{0.8}O_{3-\delta}$ Cathode Performance by Infiltration of a $Sm_{0.5}Sr_{0.5}CoO_{3-\delta}$ Coating. *Solid. State Ion.* **2009**, *180*, 1285–1289. [CrossRef]

96. Shen, F.; Lu, K. Perovskite-Type $La_{0.6}Sr_{0.4}Co_{0.2}Fe_{0.8}O_3$, $Ba_{0.5}Sr_{0.5}Co_{0.2}Fe_{0.8}O_3$, and $Sm_{0.5}Sr_{0.5}Co_{0.2}Fe_{0.8}O_3$ Cathode Materials and Their Chromium Poisoning for Solid Oxide Fuel Cells. *Electrochim. Acta* **2016**, *211*, 445–452. [CrossRef]

97. Yang, T.; Wen, Y.; Wu, T.; Xu, N.; Huang, K. A Highly Active and Cr-Resistant Infiltrated Cathode for Practical Solid Oxide Fuel Cells. *J. Mater. Chem. A Mater.* **2020**, *8*, 82–86. [CrossRef]

98. Ghorbani-Moghadam, T.; Kompany, A.; Golmohammad, M. Study of Structural, Electrical and Electrochemical Properties of $La_{0.7}Sr_{1.3}Co_{1-x}Fe_xO_4$ (x = 0, 0.1, 0.3, 0.5) Ruddlesden-Popper Oxides as Promising Cathode for Intermediate Solid Oxide Fuel Cells. *J. Alloys Compd.* **2022**, *900*, 163382. [CrossRef]

99. Liu, B.; Chen, X.; Dong, Y.; Mao, S.S.; Cheng, M. A High-Performance, Nanostructured $Ba_{0.5}Sr_{0.5}Co_{0.8}Fe_{0.2}O_{3-\delta}$ Cathode for Solid-Oxide Fuel Cells. *Adv. Energy Mater.* **2011**, *1*, 343–346. [CrossRef]

100. Yang, X.; Li, R.; Yang, Y.; Wen, G.; Tian, D.; Lu, X.; Ding, Y.; Chen, Y.; Lin, B. Improving Stability and Electrochemical Performance of $Ba_{0.5}Sr_{0.5}Co_{0.2}Fe_{0.8}O_{3-\delta}$ Electrode for Symmetrical Solid Oxide Fuel Cells by Mo Doping. *J. Alloys Compd.* **2020**, *831*, 154711. [CrossRef]

101. Zeng, Q.; Zhang, X.; Wang, W.; Zhang, D.; Jiang, Y.; Zhou, X.; Lin, B. A Zn-Doped $Ba_{0.5}Sr_{0.5}Co_{0.8}Fe_{0.2}O_{3-\delta}$ Perovskite Cathode with Enhanced ORR Catalytic Activity for SOFCs. *Catalysts* **2020**, *10*, 235. [CrossRef]

102. Nie, Z.; Wang, J.; Xia, T.; Wang, G. A-Site Ca-Doped Layered Double Perovskite $Pr_{1-x}Ca_xBa_{0.94}Co_2O_{5+\delta}$ as High-Performance and Stable Cathode for Intermediate-Temperature Solid Oxide Fuel Cells. *J. Alloys Compd.* **2022**, *905*, 164191. [CrossRef]

103. Chen, R.Y.; Zhou, D.F.; Zhu, X.F.; Wang, N.; Bai, J.H.; Guo, C.Q.; Ai, L. A Promising Nb-Doped $La_{0.5}Sr_{0.5}Co_{0.8}Cu_{0.2}O_{3-\delta}$ Cathode Materials for Intermediate Temperature Solid Oxide Fuel Cells. *J. Alloys Compd.* **2022**, *924*, 166526. [CrossRef]

104. Li, Q.; Xia, T.; Sun, L.; Zhao, H.; Huo, L. Electrochemical Performance of Novel Cobalt-Free Perovskite $SrFe_{0.7}Cu_{0.3}O_{3-\delta}$ Cathode for Intermediate Temperature Solid Oxide Fuel Cells. *Electrochim. Acta* **2014**, *150*, 151–156. [CrossRef]

105. Wu, M.; Cai, H.; Jin, F.; Sun, N.; Xu, J.; Zhang, L.; Han, X.; Wang, S.; Su, X.; Long, W.; et al. Assessment of Cobalt–Free Ferrite–Based Perovskite $Ln_{0.5}Sr_{0.5}Fe_{0.9}Mo_{0.1}O_{3-\delta}$ (Ln = lanthanide) as Cathodes for IT-SOFCs. *J. Eur. Ceram. Soc.* **2021**, *41*, 2682–2690. [CrossRef]

106. Li, L.; Jin, F.; Shen, Y.; He, T. Cobalt-Free Double Perovskite Cathode $GdBaFeNiO_{5+\delta}$ and Electrochemical Performance Improvement by $Ce_{0.8}Sm_{0.2}O_{1.9}$ Impregnation for Intermediate-Temperature Solid Oxide Fuel Cells. *Electrochim. Acta* **2015**, *182*, 682–692. [CrossRef]

107. Yu, X.; Long, W.; Jin, F.; He, T. Cobalt-Free Perovskite Cathode Materials $SrFe_{1-x}Ti_xO_{3-\delta}$ and Performance Optimization for Intermediate-Temperature Solid Oxide Fuel Cells. *Electrochim. Acta* **2014**, *123*, 426–434. [CrossRef]

108. Wang, P.; Qian, W.; Liang, H.; Zhu, X.; Cheng, J. Preparation and Electrical Properties of Cathode Material Based on Zinc-Doped $Sr_2Fe_{1.5}Mo_{0.5}O_6$ for Solid Oxide Fuel Cells. *J. Mater. Sci. Mater. Electron.* **2022**, *33*, 21660–21665. [CrossRef]

109. Kim, D.; Lee, K.T. Effect of Lanthanide (Ln = La, Nd, and Pr) Doping on Electrochemical Performance of $Ln_2NiO_{4+\delta}-YSZ$ Composite Cathodes for Solid Oxide Fuel Cells. *Ceram. Int.* **2021**, *47*, 2493–2498. [CrossRef]

110. Dąbrowa, J.; Stępień, A.; Szymczak, M.; Zajusz, M.; Czaja, P.; Świerczek, K. High-entropy approach to double perovskite cathode materials for solid oxide fuel cells: Is multicomponent occupancy in $(La,Pr,Nd,Sm,Gd)BaCo_2O_{5+\delta}$ affecting physicochemical and electrocatalytic properties? *Front. Energy Res.* **2022**, *10*, 899308. [CrossRef]

111. Liu, C.; Sun, L.; Li, Q.; Huo, L.; Zhao, H. Doping effects of alkaline earth element on oxygen reduction property of high-entropy perovskite cathode for solid oxide fuel cells. *J. Electroanal. Chem.* **2023**, *941*, 117546. [CrossRef]

112. Lu, X.; Yang, Q.; Li, R.; Zhu, S.; Zhang, J.; Liu, D.; Tian, D.; Ding, Y.; Ling, Y. High entropy engineering construction of high active and stable hybrid structure cathodes for advanced ceramic membrane fuel cells. *Fuel* **2024**, *364*, 131099. [CrossRef]

113. Salman, M.; Saleem, S.; Ling, Y.; Khan, M. Improved electrochemical performance of high-entropy $La_{0.8}Sr_{0.2}FeO_3$-based IT-SOFC cathode. *Ceram. Int.* **2024**, *50*, 39475–39484. [CrossRef]

114. Xu, Q.; Guo, Z.; Xia, L.; He, Q.; Li, Z.; Bello, I.T.; Zheng, K.; Ni, M. A comprehensive review of solid oxide fuel cells operating on various promising alternative fuels. *Energy Convers. Manag.* **2022**, *253*, 115175. [CrossRef]

115. Dou, Y.; Sun, L.; Ren, J.; Dong, L. Opportunities and Future Challenges in Hydrogen Economy for Sustainable Development. In *Hydrogen Economy: Supply Chain, Life Cycle Analysis and Energy Transition for Sustainability*; Academic Press: Cambridge, MA, USA, 2017; pp. 277–305. [CrossRef]

116. Nikolaidis, P.; Poullikkas, A. A Comparative Overview of Hydrogen Production Processes. *Renew. Sustain. Energy Rev.* **2017**, *67*, 597–611. [CrossRef]

117. Yang, B.C.; Koo, J.; Shin, J.W.; Go, D.; Shim, J.H.; An, J. Direct Alcohol-Fueled Low-Temperature Solid Oxide Fuel Cells: A Review. *Energy Technol.* **2018**, *7*, 5–19. [CrossRef]

118. Wang, W.; Qu, J.; Julião, P.S.B.; Shao, Z. Recent Advances in the Development of Anode Materials for Solid Oxide Fuel Cells Utilizing Liquid Oxygenated Hydrocarbon Fuels: A Mini Review. *Energy Technol.* **2018**, *7*, 33–44. [CrossRef]

119. Wan, Z.; Tao, Y.; Shao, J.; Zhang, Y.; You, H. Ammonia as an Effective Hydrogen Carrier and a Clean Fuel for Solid Oxide Fuel Cells. *Energy Convers. Manag.* **2021**, *228*, 113729. [CrossRef]

120. Mogensen, M.; Kammer, K. Conversion of Hydrocarbons in Solid Oxide Fuel Cells. *Annu. Rev. Mater. Res.* **2003**, *33*, 321–331. [CrossRef]

121. Park, S.; Vohs, J.M.; Gorte, R.J. Direct Oxidation of Hydrocarbons in a Solid-Oxide Fuel Cell. *Nature* **2000**, *404*, 265–267. [CrossRef]

122. Duan, C.; Kee, R.J.; Zhu, H.; Karakaya, C.; Chen, Y.; Ricote, S.; Jarry, A.; Crumlin, E.J.; Hook, D.; Braun, R.; et al. Highly Durable, Coking and Sulfur Tolerant, Fuel-Flexible Protonic Ceramic Fuel Cells. *Nature* **2018**, *557*, 217–222. [CrossRef]

123. Zhang, H.; Liu, W.; Wang, Y.; Wang, J.; Yang, J.; Liang, T.; Yin, C.; Chi, B.; Jia, L.; Guan, W. Performance and Long-Term Durability of Direct-Methane Flat-Tube Solid Oxide Fuel Cells with Symmetric Double-Sided Cathodes. *Int. J. Hydrogen Energy* **2019**, *44*, 28947–28957. [CrossRef]

124. Garcia-Garcia, F.J.; Yubero, F.; González-Elipe, A.R.; Lambert, R.M. Microstructural Engineering and Use of Efficient Poison Resistant Au-Doped Ni-GDC Ultrathin Anodes in Methane-Fed Solid Oxide Fuel Cells. *Int. J. Hydrogen Energy* **2018**, *43*, 885–893. [CrossRef]

125. Xie, Y.; Shi, N.; Hu, X.; Liu, M.; Yang, Y.; Huan, D.; Pan, Y.; Peng, R.; Xia, C. Novel In-Situ MgO Nano-Layer Decorated Carbon-Tolerant Anode for Solid Oxide Fuel Cells. *Int. J. Hydrogen Energy* **2020**, *45*, 11791–11801. [CrossRef]

126. Lee, D.; Myung, J.; Tan, J.; Hyun, S.H.; Irvine, J.T.S.; Kim, J.; Moon, J. Direct Methane Solid Oxide Fuel Cells Based on Catalytic Partial Oxidation Enabling Complete Coking Tolerance of Ni-Based Anodes. *J. Power Sources* **2017**, *345*, 30–40. [CrossRef]

127. Wang, J.; Fan, D.; Yu, L.; Wei, T.; Hu, X.; Ye, Z.; Wang, Z.; Wang, Y.; Li, C.; Yao, J.; et al. Efficient Conversion of Methane into Power via Microchanneled Solid Oxide Fuel Cells. *J. Power Sources* **2020**, *453*, 227848. [CrossRef]

128. Chen, Y.; Lu, M.; Yang, H.; Yao, Y.; Tao, T.; Lu, S.; Wang, C.; Ramesh, R.; Kendall, M.; Kendall, K.; et al. 80 Hours Operation of a Tubular Solid Oxide Fuel Cell Using Propane/Air. *Appl. Energy* **2020**, *272*, 115099. [CrossRef]

129. Yang, L.; Choi, Y.; Qin, W.; Chen, H.; Blinn, K.; Liu, M.; Liu, P.; Bai, J.; Tyson, T.A.; Liu, M. Promotion of Water-Mediated Carbon Removal by Nanostructured Barium Oxide/Nickel Interfaces in Solid Oxide Fuel Cells. *Nat. Commun.* **2011**, *2*, 357. [CrossRef]

130. Liu, M.; Choi, Y.M.; Yang, L.; Blinn, K.; Qin, W.; Liu, P.; Liu, M. Direct Octane Fuel Cells: A Promising Power for Transportation. *Nano Energy* **2012**, *1*, 448–455. [CrossRef]

131. Liu, S.; Behnamian, Y.; Chuang, K.T.; Liu, Q.; Luo, J.L. A-Site Deficient $La_{0.2}Sr_{0.7}TiO_{3-\delta}$ Anode Material for Proton Conducting Ethane Fuel Cell to Cogenerate Ethylene and Electricity. *J. Power Sources* **2015**, *298*, 23–29. [CrossRef]

132. Palo, D.R.; Dagle, R.A.; Holladay, J.D. Methanol Steam Reforming for Hydrogen Production. *Chem. Rev.* **2007**, *107*, 3992–4021. [CrossRef]

133. Liu, M.; Peng, R.; Dong, D.; Gao, J.; Liu, X.; Meng, G. Direct Liquid Methanol-Fueled Solid Oxide Fuel Cell. *J. Power Sources* **2008**, *185*, 188–192. [CrossRef]

134. Ru, Y.; Sang, J.; Xia, C.; Wei, W.C.J.; Guan, W. Durability of Direct Internal Reforming of Methanol as Fuel for Solid Oxide Fuel Cell with Double-Sided Cathodes. *Int. J. Hydrogen Energy* **2020**, *45*, 7069–7076. [CrossRef]

135. Jang, D.Y.; Koo, J.; Choi, H.R.; Kim, J.W.; Jeong, H.J.; Prinz, F.B.; Shim, J.H. Coke-Free Oxidation of Methanol in Solid Oxide Fuel Cells with Heterogeneous Nickel-Palladium Catalysts Prepared by Atomic Layer Deposition. *ACS Sustain. Chem. Eng.* **2020**, *8*, 10529–10535. [CrossRef]

136. Liang-Liang, S.; Liu, L.-L.; Luo, L.-H.; Ye-Fan, W.U.; Shi, J.-J.; Liang, C.; Xu, X.U.; You-Min, G. Facile Synthesis of Flower-like Pd Catalyst for Direct Ethanol Solid Oxide Fuel Cell. *J. Fuel Chem. Technol.* **2016**, *44*, 607–612. [CrossRef]

137. Steil, M.C.; Nobrega, S.D.; Georges, S.; Gelin, P.; Uhlenbruck, S.; Fonseca, F.C. Durable Direct Ethanol Anode-Supported Solid Oxide Fuel Cell. *Appl. Energy* **2017**, *199*, 180–186. [CrossRef]

138. Wang, W.; Su, C.; Ran, R.; Zhao, B.; Shao, Z.; Tade, M.O.; Liu, S. Nickel-Based Anode with Water Storage Capability to Mitigate Carbon Deposition for Direct Ethanol Solid Oxide Fuel Cells. *ChemSusChem* **2014**, *7*, 1719–1728. [CrossRef] [PubMed]

139. Jiang, C.; Ma, J.; Corre, G.; Jain, S.L.; Irvine, J.T.S. Challenges in Developing Direct Carbon Fuel Cells. *Chem. Soc. Rev.* **2017**, *46*, 2889–2912. [CrossRef]

140. Giddey, S.; Badwal, S.P.S.; Kulkarni, A.; Munnings, C. A Comprehensive Review of Direct Carbon Fuel Cell Technology. *Prog. Energy Combust. Sci.* **2012**, *38*, 360–399. [CrossRef]

141. Li, J.; Wei, B.; Wang, C.; Zhou, Z.; Lü, Z. High-Performance and Stable $La_{0.8}Sr_{0.2}Fe_{0.9}Nb_{0.1}O_{3-\delta}$ anode for Direct Carbon Solid Oxide Fuel Cells Fueled by Activated Carbon and Corn Straw Derived Carbon. *Int. J. Hydrogen Energy* **2018**, *43*, 12358–12367. [CrossRef]

142. Qiao, J.; Chen, H.; Wang, Z.; Sun, W.; Li, H.; Sun, K. Enhancing the Catalytic Activity of $Y_{0.08}Sr_{0.92}TiO_3$-Δ Anodes through in Situ Cu Exsolution for Direct Carbon Solid Oxide Fuel Cells. *Ind. Eng. Chem. Res.* **2020**, *59*, 13105–13112. [CrossRef]

143. Wu, H.; Xiao, J.; Zeng, X.; Li, X.; Yang, J.; Zou, Y.; Liu, S.; Dong, P.; Zhang, Y.; Liu, J. A High-Performance Direct Carbon Solid Oxide Fuel Cell—A Green Pathway for Brown Coal Utilization. *Appl. Energy* **2019**, *248*, 679–687. [CrossRef]

144. Xie, Y.; Xiao, J.; Liu, Q.; Wang, X.; Liu, J.; Wu, P.; Ouyang, S. Highly Efficient Utilization of Walnut Shell Biochar through a Facile Designed Portable Direct Carbon Solid Oxide Fuel Cell Stack. *Energy* **2021**, *227*, 120546. [CrossRef]

145. Shen, M.; Ai, F.; Ma, H.; Xu, H.; Zhang, Y. Progress and prospects of reversible solid oxide fuel cell materials. *iScience* **2021**, *24*, 103464. [CrossRef] [PubMed]

146. Kumar, S.S.; Aruna, S.T.R. Hydrocarbon Compatible SOFC Anode Catalysts and Their Syntheses: A Review. *Sustain. Chem.* **2021**, *2*, 707–763. [CrossRef]

147. Choolaei, M.; Vostakola, M.F.; Horri, B.A. Recent Advances and Challenges in Thin-Film Fabrication Techniques for Low-Temperature Solid Oxide Fuel Cells. *Crystals* **2023**, *13*, 1008. [CrossRef]

148. Oh, N.K.; Seo, J.; Lee, S.; Kim, H.-J.; Kim, U.; Lee, J.; Han, Y.-K.; Park, H. Highly efficient and robust noble-metal free bifunctional water electrolysis catalyst achieved via complementary charge transfer. *Nat. Commun.* **2021**, *12*, 4606. [CrossRef] [PubMed]

149. Thommy, L.; Benamira, M.; Jardiel, T.; Gunes, V.; Joubert, O.; Caldes, M.T. Ru exsolution in substituted $La_{0.75}Sr_{0.25}Cr_{0.5}Mn_{0.5}O_{3-\delta}$ compound as anode material for an IT-SOFCs. *Mater. Chem. Phys.* **2021**, *268*, 124724. [CrossRef]

150. Subotic, V.; Hochenauer, C. Analysis of solid oxide fuel and electrolysis cells operated in a real-system environment: State-of-the-health diagnostic, failure modes, degradation mitigation and performance regeneration. *Prog. Energy Combust. Sci.* **2022**, *93*, 101011. [CrossRef]

151. Raza, T.; Yang, J.; Wang, R.; Xia, C.; Raza, R.; Zhu, B.; Yun, S. Recent advance in physical description and material development for single component SOFC: A mini-review. *Chem. Eng. J.* **2022**, *444*, 136533. [CrossRef]

152. Zhao, F.; Peng, R.; Xia, C. A $La_{0.6}Sr_{0.4}CoO_{3-\delta}$-based electrode with high durability for intermediate temperature solid oxide fuel cells. *Mater. Res. Bull.* **2008**, *43*, 370–376. [CrossRef]

153. Park, J.-S.; Hao, N.H. Direct ethanol-fueled protonic ceramic fuel cell with reforming layer operating at low temperature. *Int. J. Hydrogen Energy* **2023**, *48*, 19207–19216. [CrossRef]

154. Petrov, A.N.; Kononchuk, O.F.; Andreev, A.V.; Cherepanov, V.A.; Kofstad, P. Crystal structure, electrical and magnetic properties of $La_{1-x}Sr_xCoO_{3-y}$. *Solid State Ion.* **1995**, *80*, 189–199. [CrossRef]